Cloud properties and their projected changes in CMIP models with low/medium/high climate sensitivity

Lisa Bock[1] and Axel Lauer[1]

[1]Deutsches Zentrum für Luft- und Raumfahrt (DLR), Institut für Physik der Atmosphäre, Oberpfaffenhofen, Germany

Correspondence: L. Bock (lisa.bock@dlr.de)

Abstract. Since the release of the first CMIP6 simulations one of the most discussed topics is the higher effective climate sensitivity (ECS) of some of the models resulting in an increased range of ECS values in CMIP6 compared to previous CMIP phases. An important contribution to ECS is the cloud climate feedback. Although climate models have continuously been developed and improved over the last decades, a realistic representation of clouds remains challenging. Clouds contribute to the large uncertainties in modeled ECS, as projected changes in cloud properties and cloud feedbacks also depend on the simulated present-day fields.

In this study we investigate the representation of both cloud physical and radiative properties from a total of 51 CMIP5 and CMIP6 models. ECS is used as a simple metric to group the models as the sensitivity of the physical cloud properties to warming is closely related to cloud feedbacks, which in turn are known to have a large contribution to ECS. Projected changes of cloud properties in future scenario simulations are analyzed by ECS group. In order to help interpreting the projected changes, model results from historical simulations are also analyzed.

The results show that differences in the net cloud radiative effect as a reaction to warming among the three model groups are driven by changes in a range of cloud regimes rather than individual regions. In polar regions, high ECS models show a weaker increase in the net cooling effect of clouds due to warming than the low ECS models. At the same time, high ECS models show a decrease in the net cooling effect of clouds over the tropical ocean and the subtropical stratocumulus regions whereas low ECS models show either little change or even an increase in the cooling effect. Over the Southern Ocean, the low ECS models show a higher sensitivity of the net cloud radiative effect to warming than the high ECS models.

1 Introduction

Climate models are an essential tool for projecting future climate. Within the context of the Coupled Model Intercomparison Project (CMIP, https://www.wcrp-climate.org/wgcm-cmip), a World Climate Research Programme (WCRP) initiative, several modeling groups worldwide provide a set of coordinated simulations with different Earth system models (ESMs) of the past (historical) time period and different future scenarios. The main objective of CMIP is to better understand past, present, and future climate, its variability and future change arising from both natural, unforced variability and in response to changes in radiative forcing in a multi-model context.

Across the different CMIP phases, several improvements e.g. in the climatological large-scale patterns of temperature, water vapor, and zonal wind speed were found with the latest phase models (CMIP6, Eyring et al. (2016)) typically performing slightly better than their CMIP3 and CMIP5 predecessors when compared to observations (Bock et al., 2020). While this is also the case for some cloud properties and selected regions such as the Southern Ocean, clouds remain challenging for global climate models with many known biases remaining in CMIP6 (Lauer et al., 2023). As such, clouds continue to play a significant role in uncertainties of climate models and climate projections (Bony et al., 2015).

One of the extensively discussed topics in analyses of the CMIP6 ensemble is the higher effective climate sensitivity (ECS) of some models and therefore the increased range in ECS now between 1.8 and 5.6 K compared to 2.1 and 4.7 in the CMIP5 ensemble (Meehl et al., 2020; Bock et al., 2020; Schlund et al., 2020). ECS provides a single number, defined as the change in global mean near-surface air temperature resulting from a doubling of the atmospheric CO_2 concentration compared to preindustrial conditions, once the climate has reached a new equilibrium (Gregory et al., 2004). A possible reason for the increase of ECS in some models is improvements in cloud representation in these models. Zelinka et al. (2020) show that the increased range of ECS in the CMIP6 models could be explained by an increased range in cloud feedbacks. Studies using single models concluded that the increased climate sensitivity found in these models is largely determined by cloud microphysical processes (Zhu et al., 2022; Frey and Kay, 2018; Gettelman et al., 2019; Bodas-Salcedo et al., 2019). They also point out that the simulated present-day mean state of cloud properties is related to the simulated cloud feedback but could also be connected to other coupled feedbacks (Andrews et al., 2019).

As future changes in cloud properties are closely connected to cloud feedbacks and cloud feedbacks are known to be strongly correlated with ECS (see Sect. 3.1), we use ECS as a simple proxy to group the ensemble of CMIP5 and CMIP6 models for this analysis. This facilitates the analysis and allows for obtaining more general conclusions beyond individual models that can vary widely in their sensitivity to the prescribed forcings. A particular focus of this study is whether there are systematic differences in cloud-related quantities between the different ECS groups. The sensitivity of the physical properties to warming is analyzed, as this gives some insight into the uncertainty of the projected cloud properties and their potential contribution to cloud feedbacks and ECS.

A comparison of the present-day climatologies of key cloud properties from the different ECS model groups is done to help interpreting simulated future changes in cloud properties. We would like to note that conclusions on the plausibility of certain ECS values cannot be drawn from this comparison and are thus not an aim of this study. The present-day performance of CMIP models has been investigated for example by Kuma et al. (2023), who applied an artificial neural network to derive cloud types from radiation fields. They found that results from models with a high ECS agree on average better with observations than from models with a low ECS. Jiang et al. (2021) found that the models' ECS is positively correlated with the integrated cloud water content and water vapor performance scores for both, CMIP6 and CMIP5 models. In contrast, Brunner et al. (2020) showed that some CMIP6 models with a high future warming compared to other models receive systematically lower performance weights when using anomaly, variance, and trend of surface air temperature, and anomaly and variance of sea level pressure to assess the models' performance.

A number of different feedbacks are relevant to ECS with cloud feedbacks being an important contribution. In order to assess whether there are systematic differences in simulated cloud properties among models with different ECS, we compare the simulated cloud properties from three groups of models sorted by their ECS values and quantify how the projected changes in cloud properties and cloud radiative effects differ. In Section 2 we briefly introduce the models and observations used as well as the software tool applied to compare the models. The representation of cloud radiative effects for all three groups is also compared with observational data in Section 3 followed by an analysis of the projected future changes in cloud properties and radiative effects. Section 4 summarizes the discussion and conclusions.

2 Data

2.1 Models

In this study we use model simulations from the CMIP Phases 5 (Taylor et al., 2012) and 6 (Eyring et al., 2016). The individual models are detailed in Table 1. All model data are freely available via the Earth System Grid Federation (ESGF), which is an international collaboration that manages the decentralized database of CMIP output.

For the analysis presented here, we use historical simulations over the time period 1985–2004 (Table 1) and the scenario simulations of the Representative Concentration Pathway (RCP) 8.5 from CMIP5 and the Shared Socioeconomic Pathways (SSP) 5-8.5 simulations from CMIP6 for the years 2081-2100. The historical simulations use prescribed natural and anthropogenic climate forcings such as concentrations of greenhouse gases and aerosols. We only consider one ensemble member per model, typically the first member "r1i1p1" (CMIP5) and "r1i1p1f1" (CMIP6). As the intermodel spread is typically much larger than the interensemble spread we do not expect our results to change significantly when using more ensemble members for each model. For further details on the model simulations, we refer to Taylor et al. (2012) and Eyring et al. (2016).

ECS and cloud feedbacks are calculated using the simulations forced by an abrupt quadrupling of CO_2 (abrupt-4×CO2) and the preindustrial control simulations (piControl) following the method described in Andrews et al. (2012) and Schlund et al. (2020).

In total, the CMIP ensemble investigated here consists of 24 CMIP5 and 27 CMIP6 models that provide the output needed for this analysis. We grouped them into the three groups "low", "medium" and "high" by their ECS values (see Table 1). The thresholds for the three groups are chosen in a way that each of the three groups contains the same number of models. Multi-model group means are calculated as 20-year means over all models in the high, medium and low ECS group applying equal weights to each model.

2.2 Observations

The Clouds and Earth's Radiant Energy Systems (CERES) Energy Balanced and Filled (EBAF) Ed4.2 dataset (Loeb et al., 2018; Kato et al., 2018) provides global monthly mean top of atmosphere (TOA) longwave (LW), shortwave (SW), and net

Table 1. List of CMIP5 and CMIP6 models grouped by ECS value into three roughly equally sized groups "high" (ECS > 4.0 K), "medium" (2.87 K < ECS < 4.0 K) and "low" (ECS < 2.87 K).

Number	CMIP5 model	CMIP6 model	ECS (K)	Citation
1		CanESM5	5.62	Swart et al. (2019)
2		HadGEM3-GC31-LL	5.55	Williams et al. (2018); Kuhlbrodt et al. (2018)
3		HadGEM3-GC31-MM	5.42	Williams et al. (2018); Kuhlbrodt et al. (2018)
4		UKESM1-0-LL	5.34	Sellar et al. (2019)
5		CESM2	5.16	Danabasoglu et al. (2020)
6		CNRM-CM6-1	4.83	Voldoire et al. (2019)
7		KACE-1-0-G	4.77	Lee et al. (2020a)
8		CNRM-ESM2-1	4.76	Séférian et al. (2019)
9		CESM2-WACCM	4.75	Danabasoglu et al. (2020)
10		NESM3	4.72	Cao et al. (2018)
11	MIROC-ESM		4.67	Watanabe et al. (2011)
12	HadGEM2-ES		4.61	Collins et al. (2011)
13		IPSL-CM6A-LR	4.56	Boucher et al. (2020)
14		TaiESM1	4.31	Lee et al. (2020b)
15	IPSL-CM5A-LR		4.13	Dufresne et al. (2013)
16	IPSL-CM5A-MR		4.12	Dufresne et al. (2013)
17	CSIRO-Mk3-6-0		4.08	Rotstayn et al. (2010)
1	GFDL-CM3		3.97	Donner et al. (2011)
2	BNU-ESM		3.92	Ji et al. (2014)
3	ACCESS1-0		3.83	Bi et al. (2013)
4	CanESM2		3.69	Arora et al. (2011)
5	MPI-ESM-LR		3.63	Giorgetta et al. (2013); Stevens et al. (2013)
6		CMCC-ESM2	3.58	Cherchi et al. (2019)
7	ACCESS1-3		3.53	Bi et al. (2013)
8		CMCC-CM2-SR5	3.52	Cherchi et al. (2019)
9	MPI-ESM-MR		3.46	Giorgetta et al. (2013); Stevens et al. (2013)
10	FGOALS-g2		3.38	Li et al. (2013)
11		MRI-ESM2-0	3.15	Yukimoto et al. (2019); Mizuta et al. (2012)
12		GISS-E2-1-H	3.11	Kelley et al. (2020)
13		BCC-CSM2-MR	3.04	Wu et al. (2019)
14		FGOALS-f3-L	3.00	He et al. (2020)
15		MPI-ESM1-2-LR	3.00	Mauritsen et al. (2019)
16		MPI-ESM1-2-HR	2.98	Muller et al. (2018)
17	CCSM4		2.94	Gent et al. (2011)
18		FGOALS-g3	2.88	Li et al. (2020)
1	bcc-csm1-1-m		2.86	Wu et al. (2010); Wu (2012)
2	bcc-csm1-1		2.83	Wu et al. (2010); Wu (2012)
3	NorESM1-M		2.80	Bentsen et al. (2013)
4		GISS-E2-1-G	2.72	Kelley et al. (2020)
5	MIROC5		2.72	Watanabe et al. (2010)
6		MIROC-ES2L	2.68	Hajima et al. (2020)
7		MIROC6	2.61	Tatebe et al. (2019)
8	IPSL-CM5B-LR		2.60	Hourdin et al. (2013)
9	MRI-CGCM3		2.60	Yukimoto et al. (2012)
10		NorESM2-LM	2.54	Seland et al. (2020)
11		NorESM2-MM	2.50	Seland et al. (2020)
12	GFDL-ESM2M		2.44	Donner et al. (2011)
13	GFDL-ESM2G		2.39	Donner et al. (2011)
14	GISS-E2-H		2.31	Schmidt et al. (2006)
15		CAMS-CSM1-0	3.29	Rong et al. (2018)
16	GISS-E2-R		2.11	Schmidt et al. (2006)
17	inmcm4		2.08	Volodin et al. (2010)

radiative fluxes under clear-sky and all-sky conditions, which are used as a reference dataset to calculate the cloud radiative

90   effects and the TOA outgoing radiation. CERES instruments are flown on NASA's Terra and Aqua satellites.

The dataset covers the whole years of the time period 2001-2022. We would like to note that the time period from the models used for comparison with the CERES-EBAF dataset (Sect. 2.1) does not match exactly the observed years. Given that ESMs are not expected to reproduce the exact observed phase of climate modes, which largely control present-day variability of clouds but rather their statistical properties, it is probably not surprising, however, that this difference in the time periods has

95   very little impact on the multi-year group averages.

Starting with CERES-EBAF Ed4.1, the dataset provides adjusted clear-sky fluxes which are now defined in a manner that is more in line with how clear-sky fluxes are represented in climate models. The uncertainty estimates for $1° \times 1°$ regional monthly net cloud radiative effects are about 7 W m^{-2} (CERES-EBAF, 2021).

2.3   ESMValTool

100   All analyses in this study are performed with the open-source community diagnostics and performance metrics tool for evaluation of ESMs "Earth System Model Evaluation Tool" (ESMValTool) version 2 (Eyring et al., 2020; Lauer et al., 2020; Righi et al., 2020; Weigel et al., 2021; Schlund et al., 2023). All figures from this paper can be reproduced by running the ESMValTool "recipe" (configuration script defining all datasets, processing steps and diagnostics) recipe_bock23acp.yml (see also the Code and Data Availability Section).

105   ## 3   Analysis

3.1   ECS and cloud feedback

The large spread in ECS of CMIP6 models could be mainly explained by uncertainties in the simulated net cloud feedback. The net cloud feedback is defined as change in the sum of shortwave and longwave cloud radiative effects at the top of the atmosphere (TOA) per degree of surface warming (2-m temperature) calculated as the difference between abrupt-4×CO2 sim-

110   ulations and the corresponding piControl simulations. The TOA shortwave and longwave cloud radiative effects are calculated as the differences between the respective TOA all-sky and clear-sky radiative fluxes. The net cloud feedback is typically dominated by the shortwave component (Zelinka et al., 2020).

The relation between ECS and simulated cloud feedbacks is illustrated in Figure 1, which shows the correlation between net, shortwave and longwave cloud feedbacks and ECS in the CMIP5 and CMIP6 models (Table 1). The relation between net

115   cloud feedback and ECS is dominated by the shortwave cloud feedback, which shows a strong correlation with ECS (r = 0.66 and a small p value of p = 3.6e-9). For the longwave cloud feedback there is only a weak (negative) correlation with ECS (p = 0.05).

As the representation of clouds and their sensitivity to climate change have a strong impact on the ECS (Zelinka et al., 2020; Bjordal et al., 2020; Bony et al., 2015) and because the range of ECS obtained from the ensemble of CMIP6 models is
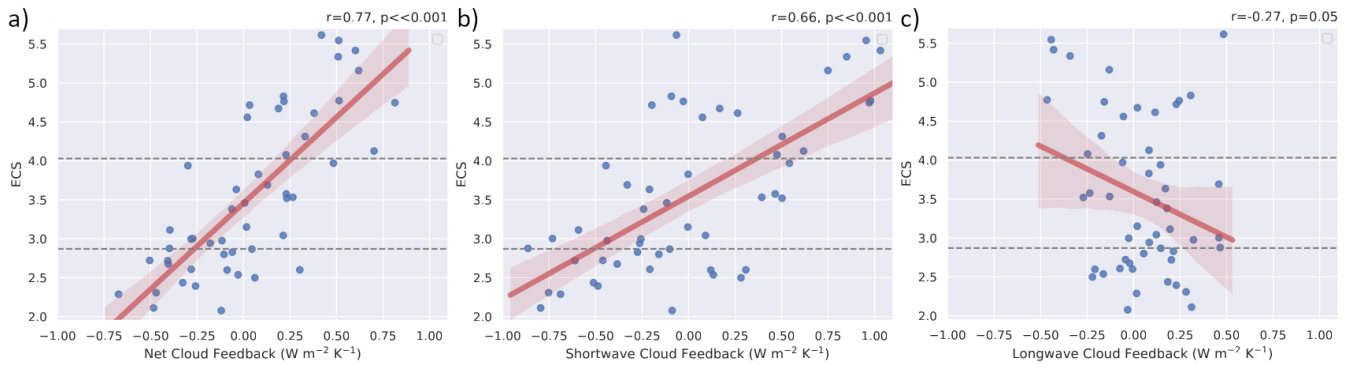
Figure 1. Scatterplot of the global mean a) net, b) shortwave and c) longwave cloud feedback (x-axis) and ECS (y-axis) of the CMIP models (Table 1) with regression line including the confidence interval of the regression of 95%. Horizontal dashed lines indicate separations of the three ECS groups (see Table 1).

larger than the one from the previous model generations (Meehl et al., 2020), this motivated us to look into the differences in present-day performance and future projections of physical cloud parameters from models with low/medium/high ECS.

Figure 2 shows the geographical distributions of the net, shortwave and longwave cloud feedbacks averaged over all models within each group. The pattern of the net cloud feedback is dominated by the geographical distribution of the shortwave cloud feedback. On global average, the high ECS group has the largest net cloud feedback of 0.41 W m^{-2}, followed by the medium ECS group (0.01 W m^{-2}) and the low ECS group (-0.20 W m^{-2}). The group mean net cloud feedback changes sign at around 60°S and 80°N in all three groups. The sign change at around 60°S in the shortwave cloud feedback corresponds to the latitude region where a change from clouds with an ice component in the piControl simulations to clouds consisting almost entirely of liquid droplets in the abrupt-4xCO2 experiment (cloud phase feedback) starts to contribute significantly to the total cloud feedback (Ceppi et al., 2017). With increasing latitude there is an increasing ice fraction in the model clouds that supports a negative shortwave feedback as cloud particles can change phase with warming. Particularly over the Arctic and the tropical Pacific, the (negative) shortwave cloud feedback is partly or fully compensated by a (positive) longwave cloud feedback resulting in rather small net cloud feedback values.

The high ECS models show a more positive net cloud feedback in the Tropics and midlatitudes, especially over the Southern Ocean, than the other two groups. The group mean of the low ECS models shows a distinct negative net cloud feedback in the Tropics, particularly in the tropical Pacific. This signal is much weaker in the other two groups. The reason is a more pronounced negative shortwave cloud feedback particularly over the Pacific Intertropical Convergence Zone (ITCZ) and South Pacific Convergence Zone (SPCZ) in the group mean of the low ECS models.

3.2 Present-day cloud fields

The representation of cloud properties in ESMs is related to the simulated cloud feedback (Zelinka et al., 2020). In order to help interpreting differences in simulated future changes in cloud properties due to warming among the three ECS groups,
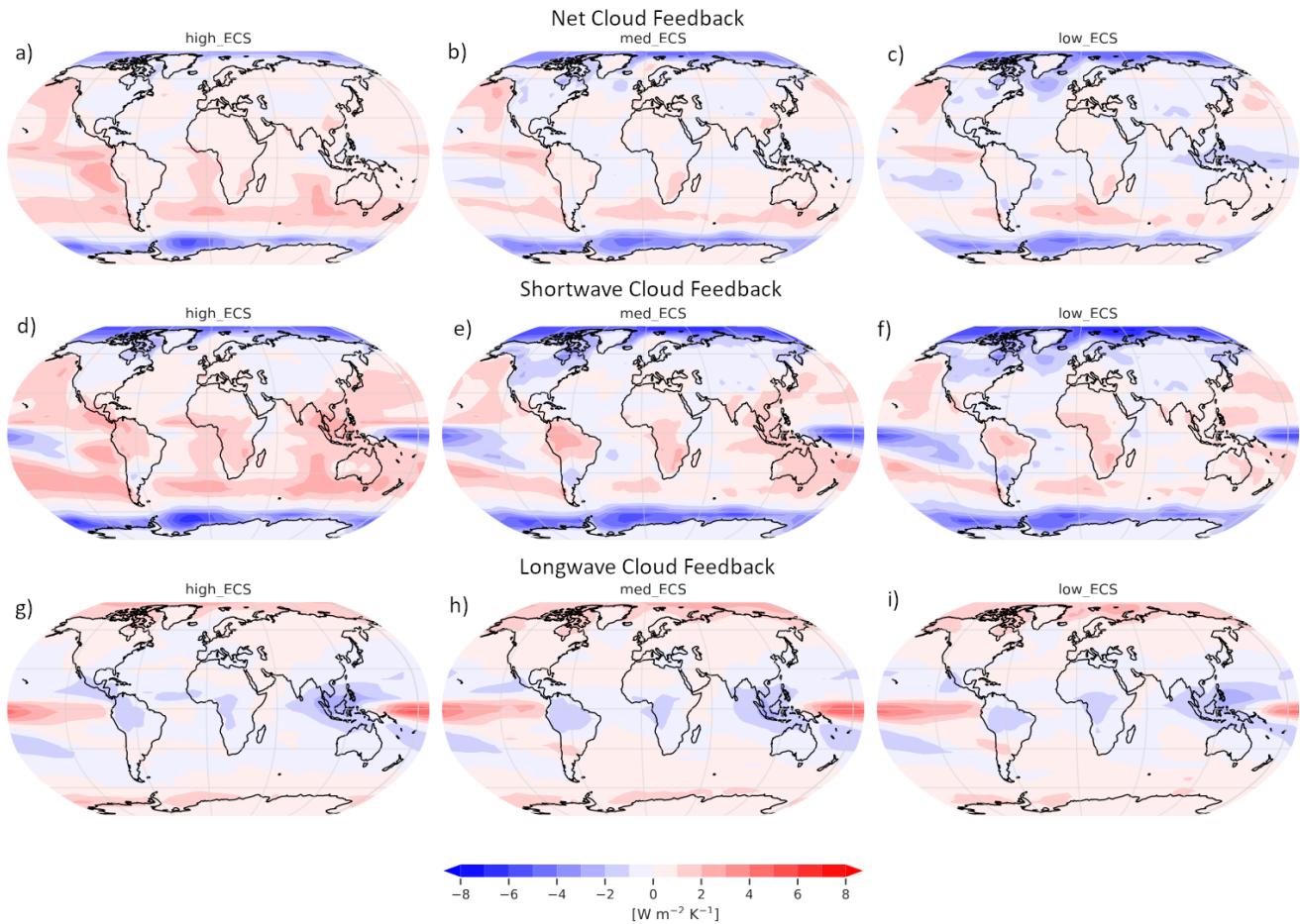
Figure 2. Geographical maps of net (a,b,c), shortwave (d,e,f) and longwave (g,h,i) cloud feedback for high (left), medium (middle) and low (right) ECS groups.

we compare the geographical distributions of the climatologies from the individual groups with each other. Here, we focus on the most climate-relevant parameters, which are total cloud fraction, liquid water and ice water path (Figure 3) and longwave, shortwave and net cloud radiative effects (Figure 4). For a direct comparison with satellite observations, output of cloud-related quantities from satellite simulators would be needed. Such output is, however, only available in very limited form or not at all from the models. Comparisons of the model results with observations are therefore restricted to cloud radiative effects, for which data are available that "were developed to be compared directly with climate model results without the need for simulators or other sampling strategies" (Loeb and NCAR Staff, 2022, see Section 2.2 for more details on CERES-EBAF).
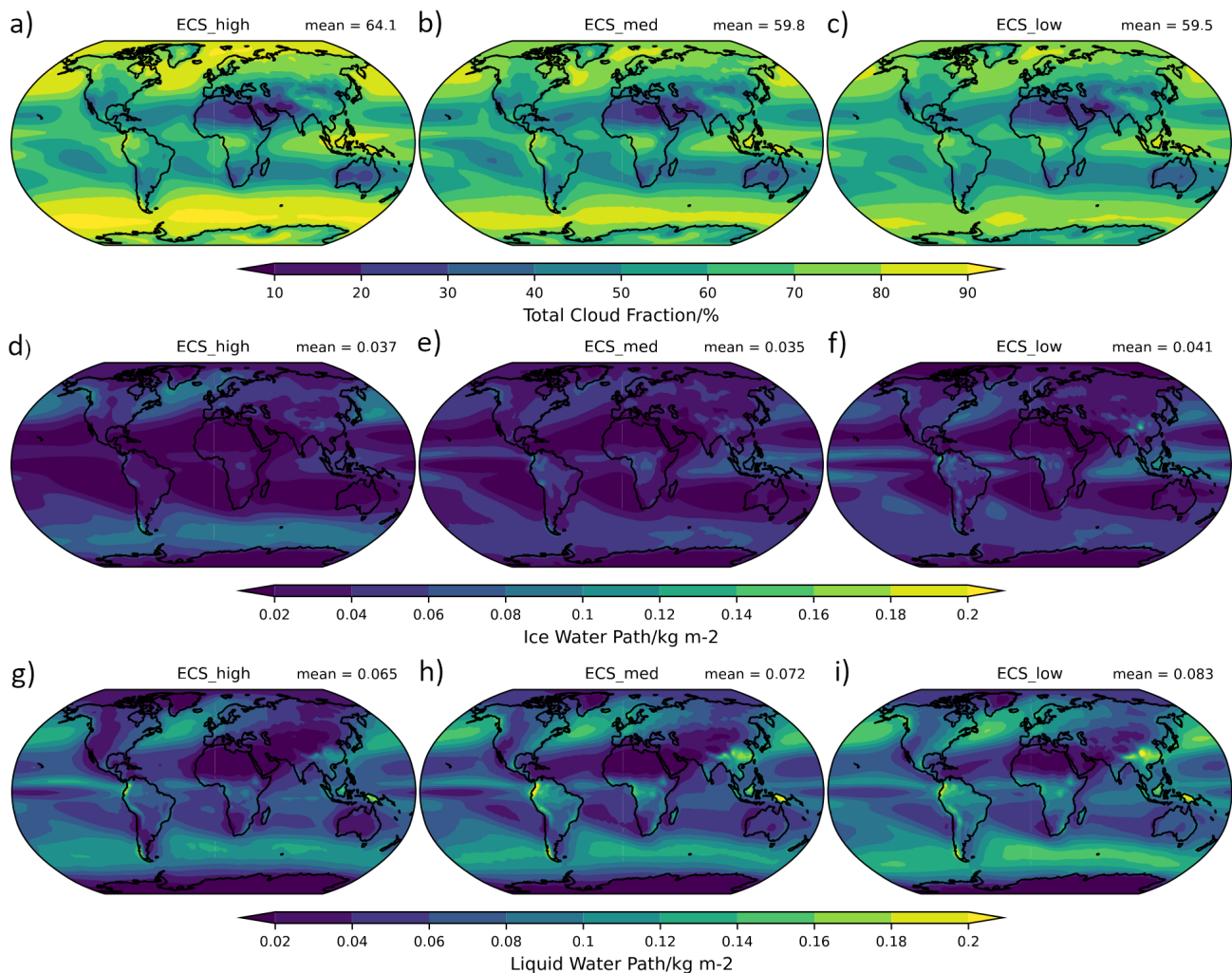
Figure 3. Geographical map of the multi-year annual mean total cloud fraction (a-c), ice water path (d-f) and liquid water path (g-i) for group means of historical CMIP simulations from all three ECS groups.

Total cloud fraction

The annual mean total cloud fraction from all ECS groups (Figure 3a-c) shows the known geographical patterns: maxima over land in the Tropics due to strong convection, minima in the subtropics because of descending air with local maxima in stratocumulus regions off the west coasts of the continents (Africa, North and South America), maxima in the midlatitudes over the ocean especially over the Southern Ocean and minima over polar regions where the air is very cold and dry.

The group mean of the high ECS models (Figure 3a) shows the largest global mean of 64.1% in total cloud cover compared to 59.8% and 59.5% for the medium and low ECS groups, respectively. Compared with the inter-model spread given by the

Table 2. Mean values of each group together with the 25% and 75% quantiles (in parentheses) calculated by bootstrapping (1000 times, sample size = number of models in the group). The second line gives the 25% and 75% quantiles calculated from all individual models.

Variable	Mean		
	high ECS	med ECS	low ECS
Total Cloud Fraction (%)	64.1 (63.3, 65.0)	59.8 (58.9, 60.0)	59.5 (59.0, 59.8)
	(61.9, 68.8)	(56.7, 62.5)	(57.8, 61.9)
Ice Water Path (g m^{-2})	37.0 (34.3, 40.1)	34.6 (30.3, 38.6)	40.7 (35.5, 45.2)
	(19.1, 51.9)	(17.6, 40.6)	(14.9, 42.3)
Liquid Water Path (g m^{-2})	65.0 (61.0, 68.5)	72.1 (67.1, 76.8)	83.2 (78.5, 87.9)
	(55.3, 68.4)	(54.6, 86.1)	(60.4, 105.5)
Net Cloud Radiative Effect (W m^{-2})	-22.8 (-23.4, -22.3)	-23.2 (-23.6, -22.8)	-25.8 (-26.3, -25.3)
	(-24.7, -20.7)	(-25.0, -21.9)	(-28.2, -23.6)

quantiles (see Table 2), this difference is a robust signal. Especially the maxima in total cloud cover over the Southern Ocean and the northern Atlantic and Pacific (Figure 3a) are more pronounced (differences up to 10%) in the group mean of the high ECS group, which leads to a slight reduction in the known bias of total cloud cover from CMIP models compared with the CMIP5/6 multi-model mean (Lauer et al., 2023). The minima polewards of about 75° are more pronounced in the low and medium ECS models (Figure 3b,c).

Ice water path

The global distribution of ice water path (Figure 3d-f) from all ECS group means shows the maximum in the ITCZ due to frequent convection of up to 0.16 kg m^{-2}. The absolute minima of ice water path are found in the subtropics in the subsidence regions west of continents. High amounts of cloud ice are also found along the stormtracks in midlatitudes, with values decreasing towards the poles.

The inter-model spread in the global mean ice water path (Table 2) is large resulting in a large overlap between the different ECS groups and no statistically significant difference in the global mean ice water path from the three ECS groups. There are, however, some differences in regional features of the ice water path distribution. The maximum of the ice water path values in the Tropics related to the ITCZ are highest in the low ECS group. In contrast, the maxima in midlatitudes, especially over the Southern Ocean, are most pronounced in the high ECS models (Figure 3d). This is consistent with the higher group mean of total cloud fraction (Figure 3a) and supports the hypothesis that the improved representation of supercooled liquid in some of the high ECS models (leading to better agreement with observations) leads to a higher ECS as it decreases the magnitude of a negative cloud phase feedback (e.g., Bock et al., 2020; Zelinka et al., 2020; Bjordal et al., 2020; Frey and Kay, 2018).

Table 3. Root mean square difference (RMSD) and pattern correlation of each group mean together with the 25% and 75% quantiles (in parentheses) calculated by bootstrapping (1000 times, sample size = number of models in the group). The second line gives the 25% and 75% quantiles calculated from all individual models. The RMSD values and the correlation are calculated in comparison to the corresponding reference dataset CERES-EBAF (see Section 2.2).

Variable	RMSD (W m^{-2})			Correlation		
	high ECS	med ECS	low ECS	high ECS	med ECS	low ECS
Net Cloud Radiative Effect	9.3 (9.0, 9.9)	9.2 (9.0, 9.7)	12.3 (11.7, 13.0)	0.86 (0.84, 0.86)	0.86 (0.85, 0.87)	0.79 (0.75, 0.80)
	(9.5, 14.1)	(10.5, 13.0)	(11.9, 18.3)	(0.74, 0.84)	(0.70, 0.82)	(0.55, 0.77)
Shortwave Cloud Radiative Effect	8.4 (8.2, 9.1)	7.8 (7.8, 8.4)	11.1 (10.7, 12.0)	0.92 (0.90, 0.92)	0.93 (0.91, 0.93)	0.87 (0.85, 0.88)
	(9.2, 13.2)	(10.6, 12.9)	(12.0, 18.5)	(0.79, 0.91)	(0.81, 0.87)	(0.73, 0.83)
Longwave Cloud Radiative Effect	5.7 (5.6, 6.1)	6.1 (6.0, 6.4)	5.9 (5.7, 6.4)	0.92 (0.91, 0.92)	0.93 (0.92, 0.93)	0.92 (0.91, 0.92)
	(7.0, 8.6)	(7.1, 8.3)	(6.3, 9.5)	(0.82, 0.87)	(0.83, 0.88)	(0.78, 0.89)

Liquid water path

The ECS group means of cloud liquid water path (Figure 3g-i) show local maxima in the ITCZ but the largest values of liquid water path are found in the extratropics in the stormtrack regions, mainly over the Southern Ocean and the northern Atlantic. There are no local maxima in the stratocumulus regions seen in all three group means which is related to a known bias of underestimating stratocumulus clouds in the CMIP models (e.g., Jian et al., 2020).

The high ECS group mean shows the lowest global mean (65.0 g m^{-2}) followed by the medium ECS group and the low ECS group with 72.1 g m^{-2} and 83.2 g m^{-2}, respectively. This negative correlation between the group-averaged global mean liquid water path and ECS seems quite robust regarding the relatively small inter-model spread in these two variables within each group. The relative differences between the ECS groups are uniformly distributed with no region being particularly pronounced.

Cloud radiative effects

The cloud radiative effects are calculated as the differences in top of the atmosphere clear-sky and all-sky radiative fluxes (for details see Secion 3.1). The CERES-EBAF data show a global mean net cooling due to clouds of about -18 W m^{-2} (Figure 4a). Clouds have a warming radiative effect in particular over regions with a high surface albedo like ice-covered regions in Greenland and Antarctica and the desert regions in North Africa. A large negative (cooling) net radiative effect of clouds is found over the stratocumulus regions in the subtropics and in the midlatitude stormtrack regions. In the ITCZ there is a partly compensating effect between the shortwave and longwave radiative effects leading to smaller absolute net values than in the stratocumulus and stormtrack regions.

Compared with CERES-EBAF, the amplitude of the global mean net cloud radiative effect is slightly overestimated in the models with the largest bias in the low ECS group (mean bias = -4.8 W m^{-2}, RMSD = 12.3 W m^{-2}) and the smallest bias in the high ECS group (mean bias = -1.8 W m^{-2}, RMSD = 9.3 W m^{-2}) (see also Table 3). While the global mean biases of the group means are within the observational uncertainty range, the RMSD values are larger than the ones of different individual
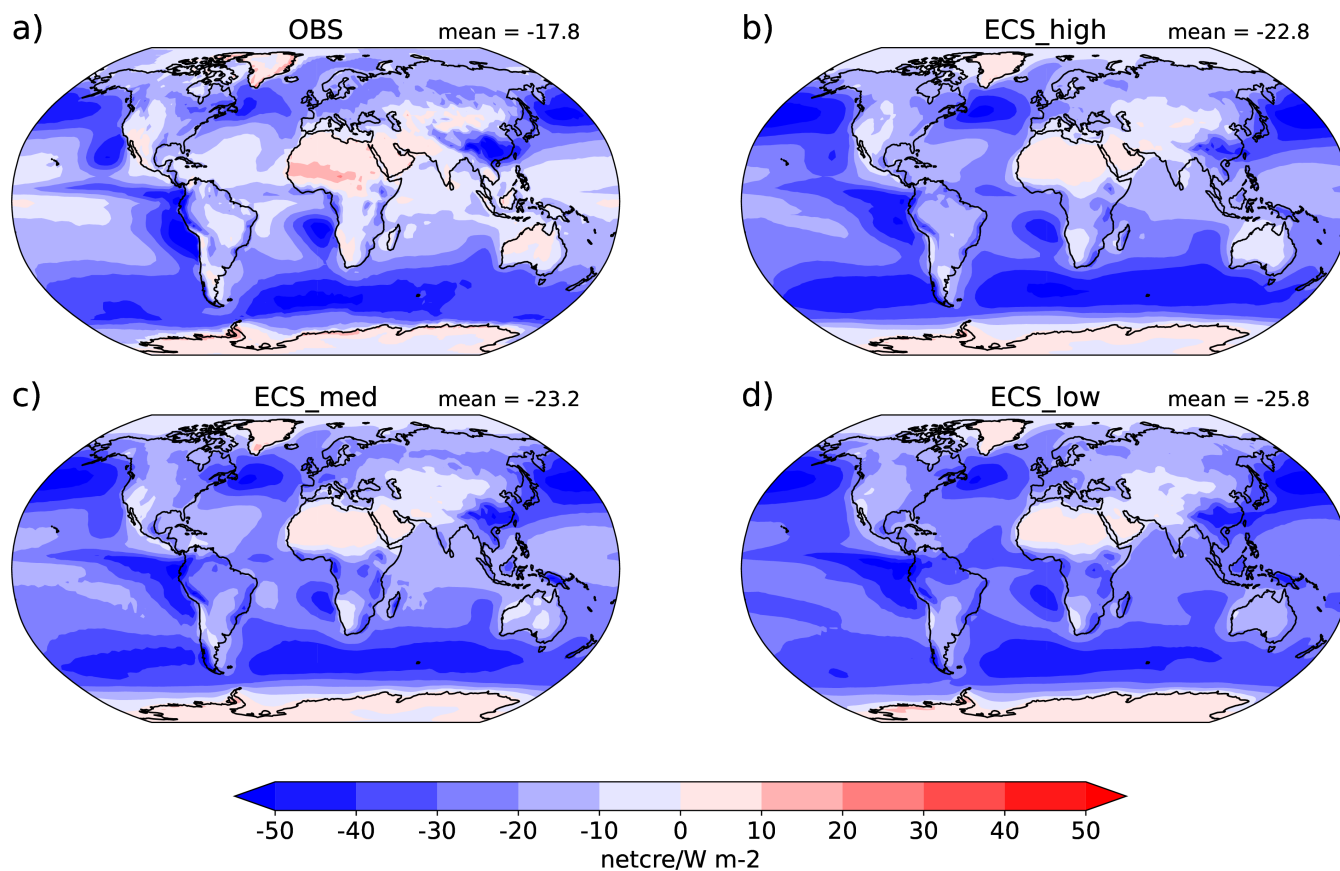
Figure 4. Geographical map of the multi-year annual mean net cloud radiative effect from (a) CERES-EBAF Ed4.2 (OBS) and (b,c,d) group means of historical CMIP simulations from all three ECS groups.

observational datasets when compared to a reference dataset consisting of an average over different products (Lauer et al., 2023).

Biases in simulated sea surface temperatures (SSTs) can affect simulated cloud properties. We therefore also analyzed some results from AMIP simulations that use the atmosphere components of the CMIP models and for which SSTs and sea ice concentrations from observations are prescribed (not shown). Similar to previous studies (e.g., Lauer and Hamilton, 2013; Lauer et al., 2023), we found rather little differences in the multi-year climatologies of cloud properties from the models between the historical and AMIP runs analyzed here.

The geographical patterns of the three model groups agree well with the CERES-EBAF observations (Figure 4). The linear pattern correlations of the annual average net cloud radiative effect from the high and the medium ECS group means with observations are slightly higher (0.86) than that of the low (0.79) ECS group. This is also reflected in the range of correlation

values from the individual models in each group given by the 25% and 75% quantiles. These range lies between 0.55 and 0.77 in the low ECS group, between 0.70 and 0.82 in the medium ECS group and between 0.74 and 0.84 in the high ECS group. For comparison, the range of correlation coefficients of different observational datasets is 0.98-0.99 (Lauer et al., 2023). The correlation values of the shortwave and longwave cloud radiative effects are larger for all ECS groups.

The peaks of positive cloud forcing over land over Greenland, North Africa and the west coast of North and South America are underestimated in all three groups. In these regions, however, observational uncertainties are expected to be large because of high surface albedo, topography or very low cloud cover. The largest positive bias for all groups is found over the stratocumulus regions with up to 46 W m^{-2} locally. Apart from this, the low ECS group shows particularly between 30°S and 30°N (Figure 4d), a too strong net cloud radiative effect resulting mainly from a too strong shortwave cooling of the clouds in this latitude belt (Figure 6e) seemingly caused by the largest cloud water path values of all three ECS groups (Figure 6b,c).

3.3 Differences in projected future cloud properties

In order to investigate the sensitivity of cloud parameters simulated by the three ECS groups to future warming, we compare the changes in selected cloud properties and cloud radiative effects in future simulations from each group. For CMIP6 we calculate the changes as differences between data from SSP5-8.5 and for CMIP5 from RCP8.5 and results for the respective historical simulations.

The zonally averaged group means (Figure 6a-f, upper panels) show the results from the historical and the scenario simulations for the investigated cloud properties (total cloud fraction, ice and liquid water path and cloud radiative effects) for the different ECS groups. Projected zonal mean changes per degree warming (near-surface temperature increase) are displayed in the panels below (Figure 6a-f, lower panels). Additionally, we show the sensitivity of cloud parameters from each ECS group over the ocean for selected regions. The relative changes (calculated as the differences between the scenario value and the historical value divided by the historical value) in cloud parameters per degree warming averaged over selected regions (Figure 5) are shown in Figure 7: 1) Arctic, 2) Southern Ocean, 3) tropical ocean, 4) Pacific ITCZ and the stratocumulus regions 5a) South East Pacific, 5b) South East Atlantic and 5c) North East Pacific.

In the following, we discuss the differences in projected future cloud properties for each cloud parameter.

Total cloud cover

For zonal mean cloud cover (Figure 6a), the comparison of the historical runs with the scenario simulations shows an increase in the zonal mean cloud cover in particular over the polar regions north and south of about 70°. This positive sensitivity to warming shows maximum values ranging between about 0.5% K^{-1} for the high, about 1% K^{-1} for the medium and 1.4% K^{-1} for the low ECS groups.

Particularly in the Tropics and in SH mid- and high latitudes, the sensitivity of simulated cloud cover to warming is quite different among the high ECS group and the two other groups. While the low and medium ECS groups show a mostly positive sensitivity in the Tropics, the high ECS group shows a negative sensitivity of cloud cover to warming of about 0.5 to -1.5% K^{-1}. Averaged over the tropical ocean (Figure 7c), the behavior of the high ECS models is significantly different than that of
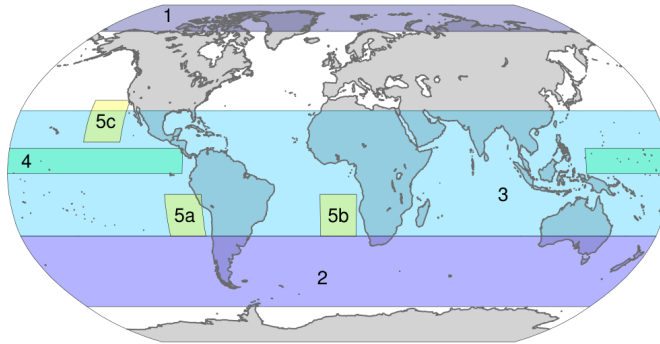
Figure 5. Maps of selected regions: 1) Arctic (70-90°N), 2) Southern Ocean (30-65°S), 3) Tropical Ocean (30°N-30°S), 4) Pacific ITCZ (0-12°N, 135°O-85°W) and the three stratocumulus regions 5a) South East Pacific (10-30°S, 75-95°W), 5b) South East Atlantic (10-30°S, 10°W-10°O) and 5c) North East Pacific (15-35°N, 120-140°W).

the two other groups. All high ECS models show a decrease in total cloud cover over the tropical ocean while the individual models in the two other groups do not agree on the sign of the change.

In all three subtropical stratocumulus regions investigated (North East Pacific, South East Pacific and South East Atlantic), 240 the high ECS group shows a decrease in total cloud cover (Figure 7e). In contrast, the low and medium ECS groups show particularly in the Southern Hemisphere stratocumulus regions an increase in total cloud cover that is most pronounced in the low ECS group.

In general, there is a decrease in cloud fraction in midlatitudes which is most pronounced in the high ECS group and becomes weaker towards the poles. In SH mid- and high latitudes south of 45°S, the low ECS group shows a strong positive sensitivity 245 of up to more than 1% K^{-1} while the high ECS group shows a negative sensitivity of about -1% K^{-1} at 45°S. South of 55°S, the high ECS group also shows a positive sensitivity of total cloud cover. The medium ECS group lies in between the low and high ECS groups but is in general closer to the low ECS group. Averaged over the Southern Ocean (latitude belt 30-65°S), the high ECS models mostly show a negative sensitivity while the individual models in the two other groups show positive and negative sensitivities.

250 **Cloud liquid and ice water path**

In the Tropics between about 10°S and 10°N, the cloud ice water path shows a strong sensitivity to warming of up to 9% K^{-1} and 10% K^{-1} in all three ECS groups (Figure 6b). The zonally averaged ice water path increases also in all three groups north and south of about 60°N/S with the high ECS group showing the strongest sensitivity to warming. Particularly in the Arctic north of 80°N, the sensitivity of the simulated ice water path to warming is about twice as high in the high ECS group (4% 255 K^{-1}) than in the medium and low ECS groups (2% K^{-1}). In midlatitudes, all groups show a negative sensitivity to warming with the high ECS group typically showing the strongest sensitivity in the Northern Hemisphere among the three ECS groups.
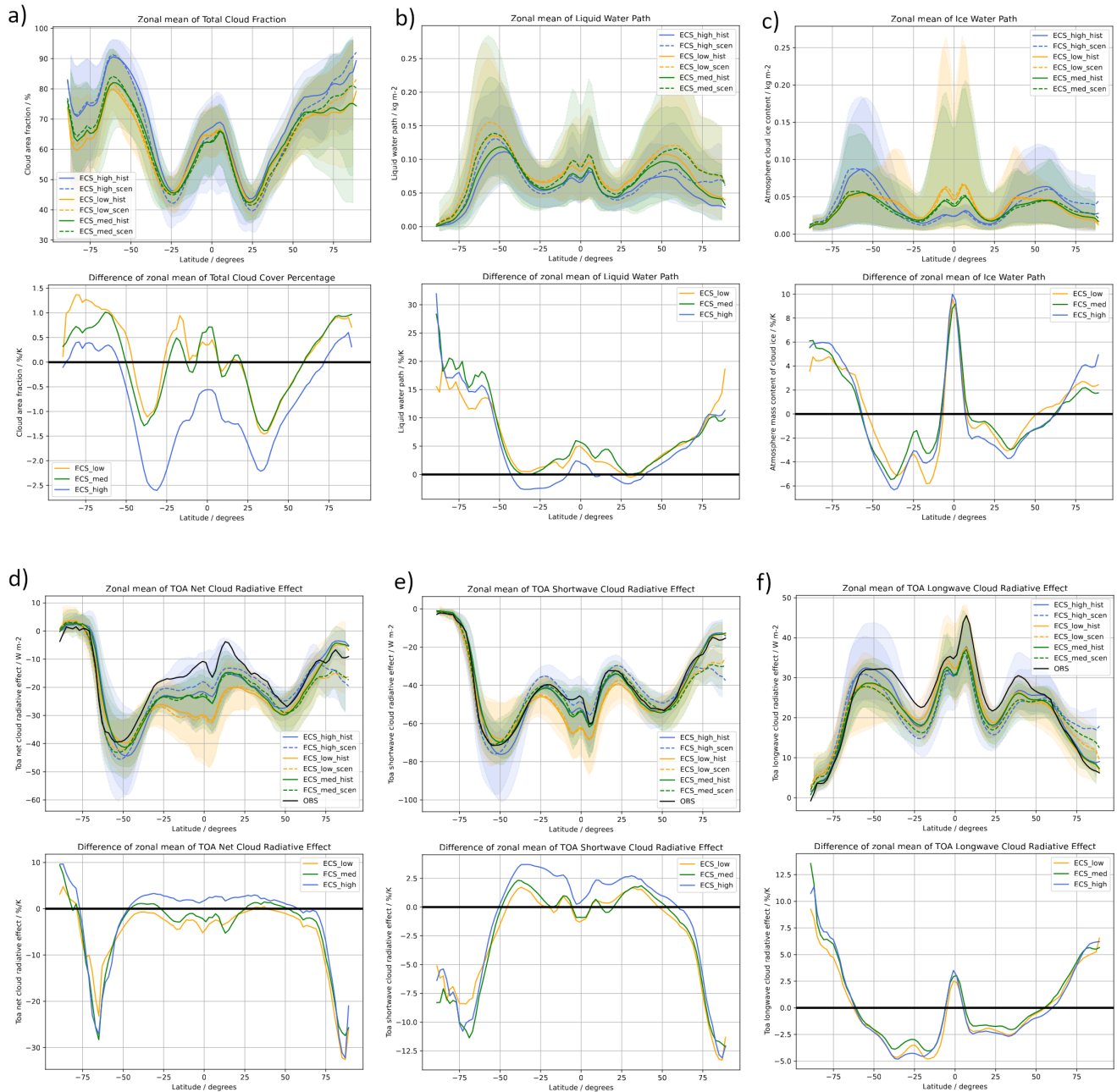
Figure 6. Upper panels: zonally averaged group means of (a) total cloud fraction, (b) liquid water path, (c) ice water path and (d) net, (e) shortwave and (f) longwave cloud radiative effect from historical simulations (solid lines) and RCP8.5 / SSP5-8.5 scenarios (dashed lines) for the three different ECS groups. The reference dataset CERES-EBAF Ed4.2 is shown as solid black lines in panels d-f. Lower panels: corresponding relative differences of all zonally averaged group means between the RCP8.5 / SSP5-8.5 scenarios and the corresponding historical simulations. Shading indicates the 5% and 95% quantiles of the single model results.
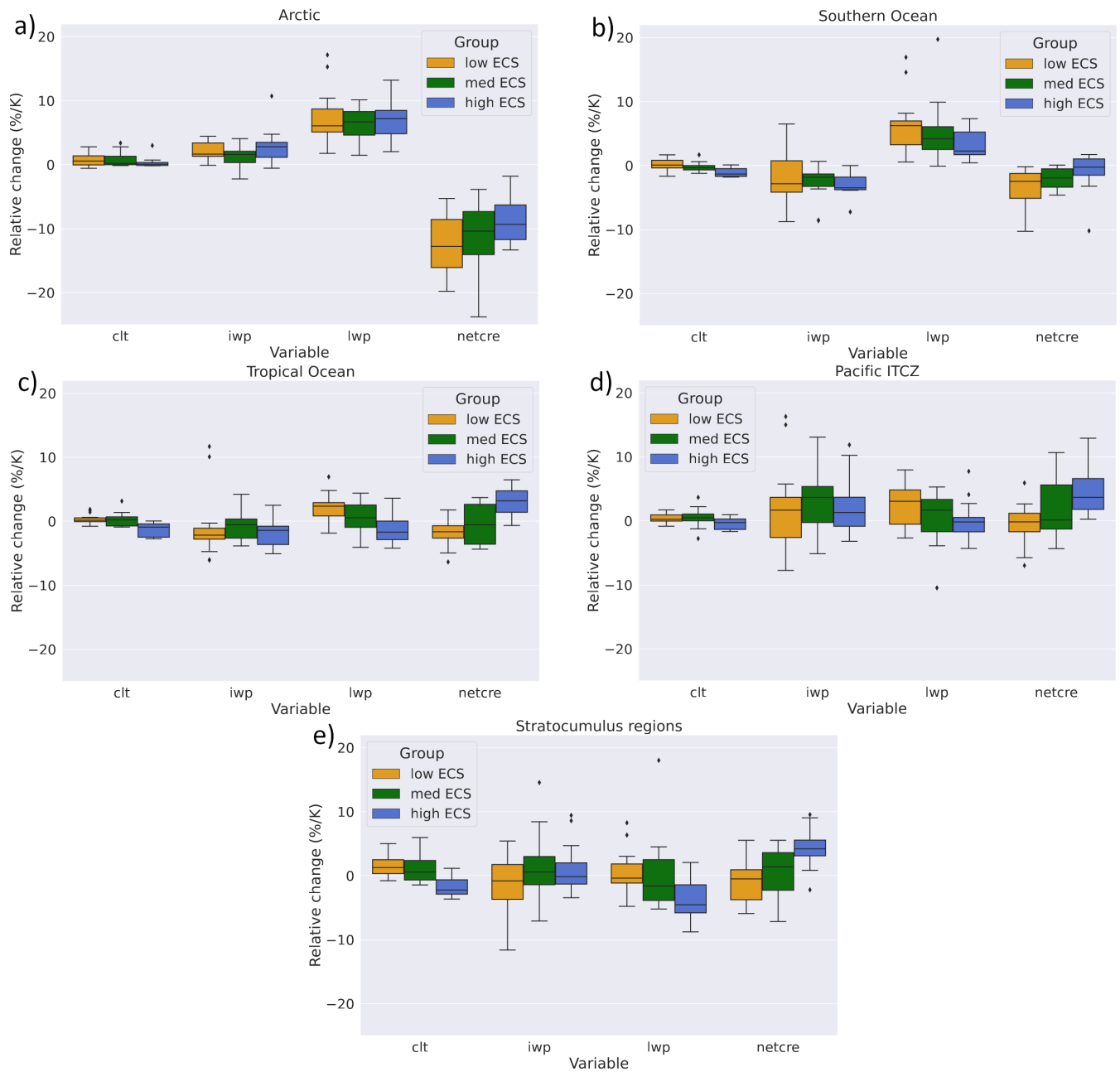
Figure 7. Relative change (calculated as the difference between the scenario value and the historical value divided by the historical value) of total cloud fraction (clt), ice water path (iwp), liquid water path (lwp) and net cloud radiative effect (netcre) per degree warming averaged over selected regions over the ocean: (a) Arctic (70-90°N), (b) Southern Ocean (30-65°S), (c) tropical ocean (30°N-30°S), (d) Pacific ITCZ (0-12°N, 135°O-85°W) and e) the three stratocumulus regions South East Pacific (10-30°S, 75-95°W), South East Atlantic (10-30°S, 10°W-10°O) and North East Pacific (15-35°N, 120-140°W) (see also Figure 5). In the box plot, each box indicates the range from the first quartile to the third quartile, the vertical line shows the median and the whiskers the minimum and maximum values excluding the outliers. Outliers are defined as being outside 1.5 times the interquartile range.

Similarly to the ice water path, also the zonally averaged liquid water path increases with temperature in all three groups in the polar regions (Figure 6c). This is consistent with the findings of Lelli et al. (2023) who report an observed trend to brighter and more liquid clouds in satellite measurements over the Arctic. In contrast to the ice water path, the lowest ECS group shows the highest sensitivity in the Arctic latitude belt. Averaged over the whole Arctic, however, there are no significant differences in ice and liquid water path over the ocean between the different ECS groups (Figure 7a).

The amplitude of the decrease in ice water path per degree warming is peaking at about 35°S and N and is about twice as large in the Southern Hemisphere than in the Northern Hemisphere. Beyond about 60°N and S, there is an increase in ice water path that is getting more pronounced towards the poles. This increase in ice water path with warming is even stronger for the liquid water path with no significant differences between the ECS groups. This increase in liquid water path can be partly explained by a phase change from cloud ice to liquid at higher temperatures.

In the stratocumulus regions (Figure 7e), liquid water path increases in the low ECS model group while it decreases in the high ECS group. The medium ECS group lies in between the two with many of the individual models disagreeing on the sign of the change. This behavior is consistent with the sensitivity of the changes in total cloud cover in these regions. We would like to note that ice water path values are typically very small in the stratocumulus regions. Relative changes can therefore be large without being physically relevant.

Over the Southern Ocean, the decrease in ice water path and the increase in liquid water path with warming is also not statistically significantly different among the three ECS groups. Averaged over the whole Southern Ocean (Figure 7b), all high ECS models show a decrease in cloud ice water path whereas about half of the low ECS models show an increase.

Cloud radiative effects

Over the northern polar region the cooling effect of the net cloud radiative effect increases significantly for all three ECS groups (Figure6def). Averaged over the whole Arctic (Figure 7a), the low ECS group shows the strongest increase in cooling among the three ECS groups. The increase in net cloud radiative effect is dominated by a stronger shortwave cloud radiative effect that is only partly compensated by a larger longwave cloud radiative effect. This is driven particularly by an increase in cloud liquid water path and only to a smaller extent to an increase in cloud ice water path and total cloud cover (Figures 6abc).

North of about 50°N and south of about 50°S, all three ECS groups show stronger shortwave cloud radiative effects, i.e. stronger cooling, in the future scenarios than in the historical simulations. In contrast, the shortwave cloud radiative effect is reduced in the projections in mid- and low latitudes. Here, the low ECS group shows the smallest changes, while the reductions in shortwave cloud radiative effect per degree of warming are strongest in the high ECS group. This is mainly driven by a reduction in total cloud cover alongside a reduction in liquid water path that can only be compensated within about $\pm 10°$ around the Equator by an increase in cloud ice water path (Figure 6abc).

On average, there is a small decrease in the amplitude of the net radiative effect between about 1 and 3% K^{-1} for high ECS models in the latitude belt 50°S to 50°N. For the two other groups there is a small increase in the amplitude. Beyond 50°N and 50°S the amplitude of the net cloud radiative effect increases (i.e. more negative) per degree temperature change with a peak at about 65°S and 80°N of about 25% and 30%, respectively, per degree temperature increase. Ceppi et al. (2016) shows that

this cloud response results from an increasing cloud optical depth with temperature which is in agreement with the increased liquid water path in Figure 6c.

In the Tropics, the high ECS group shows the strongest weakening of the net cloud radiative effect. This is caused by a reduced shortwave cooling (Figure 6e) connected to the decrease in total cloud fraction. In contrast, the medium and low ECS groups show a stronger net cloud radiative effect (i.e. more negative) with warming in the future projections. This different behavior can also be seen in Figure 7c.

Driven mostly by the changes in total cloud cover and liquid water path, the cooling effect of the net cloud radiative effect in the stratocumulus regions amplifies with warming in the low ECS group while it gets weaker in the high ECS group (Figure 7d). Again, the medium ECS group is in between the two other groups with many individual models within this group disagreeing on the sign of the change in the net cloud radiative effect with warming.

4 Summary and conclusions

The uncertainty in the representation of clouds and their response to climate change is one of the main contributors to the overall uncertainty in effective climate sensitivity and thus projections of future climate. The increased range of ECS obtained from the ensemble of CMIP6 models compared to previous CMIP phases motivated us to look into the differences in present-day and future projections of cloud parameters. For this, a total of 51 CMIP5 and CMIP6 models providing the required output were grouped by their ECS into three equally sized groups to investigate changes in cloud parameters in future projections from these models. Models with an ECS higher than 4.0 K belong to the "high" ECS group, with an ECS between 2.87 K and 4.0 K to the "medium" and with an ECS lower than 2.87 K to the "low" ECS group. Furthermore, historical simulations of the models were compared to each other to obtain a qualitative overview on the differences among the three model groups in simulating observed cloud patterns and properties.

We found higher total cloud cover values in the high ECS group mean with especially the maxima over the Southern Ocean and the northern Atlantic and Pacific being more pronounced. The high ECS group mean also shows the largest values of ice water path over the Southern Ocean among the three groups whereas the expected maxima of the ice water path in the Tropics related to the ITCZ are more pronounced in the low ECS group mean. The liquid water path is lowest in the low ECS group mean over the whole globe.

When comparing the group mean net cloud radiative effects to the observationally based CERES-EBAF dataset, we found the bias, RMSD and correlation to be significant worse for the low ECS group than for the two other groups. The low ECS group shows the highest overestimation of the net cloud radiative effect in the Tropics and at the same time the highest ice water path in this region among the three model groups.

In order to investigate the sensitivity of cloud parameters to future warming simulated by the three ECS groups, we compared results from historical simulations with the ones from RCP8.5 and SSP5-8.5 runs from each group. We found that in polar regions, the increase in cloud cover per degree of warming is strongest in the low ECS models, which is about a factor of 2-3 higher than in the high ECS models. Together with an increase in cloud ice and liquid water path, the cooling effect of the net

cloud radiative effect increases significantly for all three ECS groups particularly in the northern polar region. These simulated
future changes in all three groups in polar regions are consistent with satellite observations showing an increase in the observed
brightness of Arctic clouds in recent years (Lelli et al., 2023). Averaged over the whole Arctic, the low ECS group shows the
strongest increase in the cooling effect of the shortwave cloud radiative effect among the three ECS groups.

In midlatitudes and in the Tropics, the three model groups do not agree on the sign of the sensitivity of cloud cover to
warming. While the high ECS models show a decrease in cloud fraction particularly in SH mid- and high latitudes south of
45°S, the low ECS group shows a strong positive sensitivity of up to more than 1% K^{-1}. Over the tropical ocean, all high ECS
models show a decrease in total cloud cover while the individual models in the two other groups do not agree on the sign of the
change. The shortwave cloud radiative effect is reduced in the projections in mid- and low latitudes with the low ECS group
showing the smallest changes, while the reductions in shortwave cloud radiative effect per degree of warming are strongest in
the high ECS group. This is mainly driven by a reduction in total cloud cover alongside a reduction in liquid water path that
can only be compensated within about $\pm 10°$ around the Equator by an increase in cloud ice water path. Between about 10°S
and 10°N all three ECS groups show a strong sensitivity of the cloud ice water path to warming of up to 9% K^{-1} and 10%
K^{-1}. This increase in cloud ice water path is expected to be related to stronger and/or more frequent deep convection as the
main increase in the vertical distribution of cloud ice occurs in the upper troposphere around 300 hPa and higher (not shown).

Similarly, the behavior of the three ECS groups is different in the subtropical stratocumulus regions. The high ECS group
shows a decrease in total cloud cover with warming, the low and medium ECS groups show particularly in the SH stratocumulus
regions an increase in total cloud cover. Together with changes in liquid water path following changes in cloud cover, the
cooling effect of the net cloud radiative effect in the stratocumulus regions amplifies with warming in the low ECS group while
it gets weaker in the high ECS group. Failure to reproduce observed trends in sea surface temperature gradient and therefore
changes in inversion strength has found to be one possible reason for an overestimation of the positive cloud feedback in the
stratocumulus regions (Cesana and Del Genio, 2021).

Over the Southern Ocean, we found a decrease in ice water path and an increase in liquid water path with warming. These
changes, however, are not statistically significantly different among the three ECS groups. Averaged over the whole Southern
Ocean (latitude belt 30-65°S), all high ECS models agree in a future decrease in cloud ice water path whereas about half of the
low ECS models show a positive and half of the models a negative change in cloud ice. This might be connected to the higher
ice water path over the Southern Ocean of the high ECS group mean in today's climate.

Our results suggest that the differences in the net cloud radiative effect as a response to warming and thus differences in
ECS among the CMIP models are not solely driven by an individual region but rather by changes in a range of cloud regimes
leading to differences in the net cloud radiative effects. Contributors are changes in all different global cloud regimes, in polar
regions, in tropical and subtropical regions and in midlatitudes. In polar regions, high ECS models show a significantly weaker
increase in the net cooling effect of clouds due to warming than the low ECS models. At the same time, high ECS models
show a decrease in the net cooling effect of clouds over the tropical ocean and the subtropical stratocumulus regions. In both
regions low ECS models show either little change or even an increase in the cooling effect as a consequence of warming. The
differences among the ECS groups in the Southern Ocean fit consistently into this picture, showing a higher sensitivity of the

net cloud radiative effect to warming in the low ECS models than in the high ECS models. We thus conclude that changes in
360 all three regions contribute to the amplitude of simulated ECS.

Code and data availability. All model simulations used for this paper are publicly available on ESGF. The observational dataset CERES-EBAF Ed4.2 (see Section 2.2) is not distributed with the ESMValTool that is restricted to the code as open source software, but the ESMValTool provides a script with exact downloading and processing instructions to recreate the dataset used in this publication. All diagnostics used for this paper will be made available in the ESMValTool after acceptance of this publication. ESMValTool v2 is released under the Apache
365 License, version 2.0. The latest release of ESMValTool v2 is publicly available on Zenodo at https://doi.org/10.5281/zenodo.3401363. The source code of the ESMValCore package, which is installed as a dependency of the ESMValTool v2, is also publicly available on Zenodo at https://doi.org/10.5281/zenodo.3387139. ESMValTool and ESMValCore are developed on the GitHub repositories available at https://github.com/ESMValGroup with contributions from the community very welcome. For more information, we refer to the ESMValTool website (https://www.esmvaltool.org). All figures from this paper can be reproduced with the ESMValTool "recipe" (configuration script
370 defining all datasets, processing steps and diagnostics to be applied) recipe_bock23acp.yml.

Author contributions. LB performed the analysis, prepared all figures, and lead the writing of the manuscript. AL contributed to the scientific interpretation of the results and the writing of the manuscript.

Competing interests. No competing interests.

Acknowledgements. This project has received funding from the European Union's Horizon 2020 research and innovation programme un-
375 der Grant Agreement 101003536 (ESM2025—Earth System Models for the Future) and from the ESA Climate Change Initiative Climate Modelling User Group (ESA CCI CMUG).

We acknowledge the World Climate Research Programme, which, through its Working Group on Coupled Modelling, coordinated and promoted CMIP6. We thank the climate modeling groups for producing and making available their model output, the Earth System Grid Federation (ESGF) for archiving the data and providing access, and the multiple funding agencies that support CMIP6 and ESGF. This work
380 used resources of the Deutsches Klimarechenzentrum (DKRZ) granted by its Scientific Steering Committee (WLA) under project ID bd0854.

The CERES-EBAF data were obtained from the NASA Langley Research Center Atmospheric Science Data Center.

We thank Mattia Righi (DLR) and three anonymous reviewers for their helpful comments on the manuscript.

References

Andrews, T., Gregory, J. M., Webb, M. J., and Taylor, K. E.: Forcing, feedbacks and climate sensitivity in CMIP5 coupled atmosphere-ocean climate models, Geophysical Research Letters, 39, https://doi.org/10.1029/2012GL051607, 2012.

Andrews, T., Andrews, M. B., Bodas-Salcedo, A., Jones, G. S., Kulhbrodt, T., Manners, J., Menary, M. B., Ridley, J., Ringer, M. A., and Sellar, A. A.: Forcings, feedbacks and climate sensitivity in HadGEM3-GC3. 1 and UKESM1, Journal of Advances in Modeling Earth Systems, 2019.

Arora, V. K., Scinocca, J. F., Boer, G. J., Christian, J. R., Denman, K. L., Flato, G. M., Kharin, V. V., Lee, W. G., and Merryfield, W. J.: Carbon emission limits required to satisfy future representative concentration pathways of greenhouse gases, Geophys Res Lett, 38, https://doi.org/10.1029/2010gl046270, 2011.

Bentsen, M., Bethke, I., Debernard, J. B., Iversen, T., Kirkevag, A., Seland, O., Drange, H., Roelandt, C., Seierstad, I. A., Hoose, C., and Kristjansson, J. E.: The Norwegian Earth System Model, NorESM1-M - Part 1: Description and basic evaluation of the physical climate, Geosci Model Dev, 6, 687–720, https://doi.org/10.5194/gmd-6-687-2013, 2013.

Bi, D. H., Dix, M., Marsland, S. J., O'Farrell, S., Rashid, H. A., Uotila, P., Hirst, A. C., Kowalczyk, E., Golebiewski, M., Sullivan, A., Yan, H. L., Hannah, N., Franklin, C., Sun, Z. A., Vohralik, P., Watterson, I., Zhou, X. B., Fiedler, R., Collier, M., Ma, Y. M., Noonan, J., Stevens, L., Uhe, P., Zhu, H. Y., Griffies, S. M., Hill, R., Harris, C., and Puri, K.: The ACCESS coupled model: description, control climate and evaluation, Aust Meteorol Ocean Aust Meteorol Ocean, 63, 41–64, 2013.

Bjordal, J., Storelvmo, T., Alterskjær, K., and Carlsen, T.: Equilibrium climate sensitivity above 5°{C} plausible due to state-dependent cloud feedback, Nature Geoscience, 13, 718–721, https://doi.org/10.1038/s41561-020-00649-1, 2020.

Bock, L., Lauer, A., Schlund, M., Barreiro, M., Bellouin, N., Jones, C., Meehl, G. A., Predoi, V., Roberts, M. J., and Eyring, V.: Quantifying Progress Across Different CMIP Phases With the ESMValTool, Journal of Geophysical Research: Atmospheres, 125, e2019JD032 321, https://doi.org/10.1029/2019JD032321, 2020.

Bodas-Salcedo, A., Mulcahy, J. P., Andrews, T., Williams, K. D., Ringer, M. A., Field, P. R., and Elsaesser, G. S.: Strong dependence of atmospheric feedbacks on mixed-phase microphysics and aerosol-cloud interactions in HadGEM3, Journal of Advances in Modeling Earth Systems, 2019.

Bony, S., Stevens, B., Frierson, D. M. W., Jakob, C., Kageyama, M., Pincus, R., Shepherd, T. G., Sherwood, S. C., Siebesma, A. P., Sobel, A. H., Watanabe, M., and Webb, M. J.: Clouds, circulation and climate sensitivity, Nature Geoscience, 8, 261–268, https://doi.org/10.1038/ngeo2398, 2015.

Boucher, O., Servonnat, J., Albright, A. L., Aumont, O., Balkanski, Y., Bastrikov, V., Bekki, S., Bonnet, R., Bony, S., Bopp, L., Braconnot, P., Brockmann, P., Cadule, P., Caubel, A., Cheruy, F., Codron, F., Cozic, A., Cugnet, D., D'Andrea, F., Davini, P., de Lavergne, C., Denvil, S., Deshayes, J., Devilliers, M., Ducharne, A., Dufresne, J.-L., Dupont, E., Éthé, C., Fairhead, L., Falletti, L., Flavoni, S., Foujols, M.-A., Gardoll, S., Gastineau, G., Ghattas, J., Grandpeix, J.-Y., Guenet, B., Guez, E., L., Guilyardi, E., Guimberteau, M., Hauglustaine, D., Hourdin, F., Idelkadi, A., Joussaume, S., Kageyama, M., Khodri, M., Krinner, G., Lebas, N., Levavasseur, G., Lévy, C., Li, L., Lott, F., Lurton, T., Luyssaert, S., Madec, G., Madeleine, J.-B., Maignan, F., Marchand, M., Marti, O., Mellul, L., Meurdesoif, Y., Mignot, J., Musat, I., Ottlé, C., Peylin, P., Planton, Y., Polcher, J., Rio, C., Rochetin, N., Rousset, C., Sepulchre, P., Sima, A., Swingedouw, D., Thiéblemont, R., Traore, A. K., Vancoppenolle, M., Vial, J., Vialard, J., Viovy, N., and Vuichard, N.: Presentation and Evaluation of the IPSL-CM6A-LR Climate Model, Journal of Advances in Modeling Earth Systems, 12, e2019MS002 010, https://doi.org/10.1029/2019ms002010, 2020.

Brunner, L., Pendergrass, A. G., Lehner, F., Merrifield, A. L., Lorenz, R., and Knutti, R.: Reduced global warming from CMIP6 projections when weighting models by performance and independence, Earth System Dynamics, 11, 995–1012, https://doi.org/10.5194/esd-11-995-2020, 2020.

Cao, J., Wang, B., Young-Min, Y., Ma, L., Li, J., Sun, B., Bao, Y., He, J., Zhou, X., and Wu, L.: The NUIST Earth System Model (NESM) version 3: description and preliminary evaluation, Geoscientific Model Development, 11, 2975–2993, 2018.

Ceppi, P., McCoy, D. T., and Hartmann, D. L.: Observational evidence for a negative shortwave cloud feedback in middle to high latitudes, Geophysical Research Letters, 43, 1331–1339, https://doi.org/10.1002/2015GL067499, _eprint: https://agupubs.onlinelibrary.wiley.com/doi/pdf/10.1002/2015GL067499, 2016.

Ceppi, P., Brient, F., Zelinka, M. D., and Hartmann, D. L.: Cloud feedback mechanisms and their representation in global climate models, WIREs Climate Change, 8, e465, https://doi.org/10.1002/wcc.465, publisher: John Wiley & Sons, Ltd, 2017.

CERES-EBAF: CERES-EBAF Ed4.1 Data Quality Summary V3, https://ceres.larc.nasa.gov/documents/DQ_summaries/CERES_EBAF_Ed4.1_DQS.pdf, (last access on 2023-11-23), 2021.

Cesana, G. V. and Del Genio, A. D.: Observational constraint on cloud feedbacks suggests moderate climate sensitivity, Nature Climate Change, 11, 213–218, https://doi.org/10.1038/s41558-020-00970-y, 2021.

Cherchi, A., Fogli, P. G., Lovato, T., Peano, D., Iovino, D., Gualdi, S., Masina, S., Scoccimarro, E., Materia, S., and Bellucci, A.: Global Mean Climate and Main Patterns of Variability in the CMCC-CM2 Coupled Model, Journal of Advances in Modeling Earth Systems, 11, 185–209, 2019.

Collins, W. J., Bellouin, N., Doutriaux-Boucher, M., Gedney, N., Halloran, P., Hinton, T., Hughes, J., Jones, C. D., Joshi, M., Liddicoat, S., Martin, G., O'Connor, F., Rae, J., Senior, C., Sitch, S., Totterdell, I., Wiltshire, A., and Woodward, S.: Development and evaluation of an Earth-System model-HadGEM2, Geosci Model Dev, 4, 1051–1075, https://doi.org/10.5194/gmd-4-1051-2011, 2011.

Danabasoglu, G., Lamarque, J. F., Bacmeister, J., Bailey, D. A., DuVivier, A. K., Edwards, J., Emmons, L. K., Fasullo, J., Garcia, R., Gettelman, A., Hannay, C., Holland, M. M., Large, W. G., Lauritzen, P. H., Lawrence, D. M., Lenaerts, J. T. M., Lindsay, K., Lipscomb, W. H., Mills, M. J., Neale, R., Oleson, K. W., Otto-Bliesner, B., Phillips, A. S., Sacks, W., Tilmes, S., van Kampenhout, L., Vertenstein, M., Bertini, A., Dennis, J., Deser, C., Fischer, C., Fox-Kemper, B., Kay, J. E., Kinnison, D., Kushner, P. J., Larson, V. E., Long, M. C., Mickelson, S., Moore, J. K., Nienhouse, E., Polvani, L., Rasch, P. J., and Strand, W. G.: The Community Earth System Model Version 2 (CESM2), J Adv Model Earth Sy, 12, 2020.

Donner, L. J., Wyman, B. L., Hemler, R. S., Horowitz, L. W., Ming, Y., Zhao, M., Golaz, J. C., Ginoux, P., Lin, S. J., Schwarzkopf, M. D., Austin, J., Alaka, G., Cooke, W. F., Delworth, T. L., Freidenreich, S. M., Gordon, C. T., Griffies, S. M., Held, I. M., Hurlin, W. J., Klein, S. A., Knutson, T. R., Langenhorst, A. R., Lee, H. C., Lin, Y. L., Magi, B. I., Malyshev, S. L., Milly, P. C. D., Naik, V., Nath, M. J., Pincus, R., Ploshay, J. J., Ramaswamy, V., Seman, C. J., Shevliakova, E., Sirutis, J. J., Stern, W. F., Stouffer, R. J., Wilson, R. J., Winton, M., Wittenberg, A. T., and Zeng, F. R.: The Dynamical Core, Physical Parameterizations, and Basic Simulation Characteristics of the Atmospheric Component AM3 of the GFDL Global Coupled Model CM3, J Climate, 24, 3484–3519, https://doi.org/10.1175/2011jcli3955.1, 2011.

Dufresne, J. L., Foujols, M. A., Denvil, S., Caubel, A., Marti, O., Aumont, O., Balkanski, Y., Bekki, S., Bellenger, H., Benshila, R., Bony, S., Bopp, L., Braconnot, P., Brockmann, P., Cadule, P., Cheruy, F., Codron, F., Cozic, A., Cugnet, D., de Noblet, N., Duvel, J. P., Ethe, C., Fairhead, L., Fichefet, T., Flavoni, S., Friedlingstein, P., Grandpeix, J. Y., Guez, L., Guilyardi, E., Hauglustaine, D., Hourdin, F., Idelkadi, A., Ghattas, J., Joussaume, S., Kageyama, M., Krinner, G., Labetoulle, S., Lahellec, A., Lefebvre, M. P., Lefevre, F., Levy, C., Li, Z. X., Lloyd, J., Lott, F., Madec, G., Mancip, M., Marchand, M., Masson, S., Meurdesoif, Y., Mignot, J., Musat, I., Parouty, S., Polcher, J.,

Rio, C., Schulz, M., Swingedouw, D., Szopa, S., Talandier, C., Terray, P., Viovy, N., and Vuichard, N.: Climate change projections using the IPSL-CM5 Earth System Model: from CMIP3 to CMIP5, Clim Dynam, 40, 2123–2165, https://doi.org/10.1007/s00382-012-1636-1, 2013.

460 Eyring, V., Bony, S., Meehl, G. A., Senior, C. A., Stevens, B., Stouffer, R. J., and Taylor, K. E.: Overview of the Coupled Model Intercomparison Project Phase 6 (CMIP6) experimental design and organization, Geosci Model Dev, 9, 1937–1958, https://doi.org/10.5194/gmd-9-1937-2016, 2016.

Eyring, V., Bock, L., Lauer, A., Righi, M., Schlund, M., Andela, B., Arnone, E., Bellprat, O., Brotz, B., Caron, L. P., Carvalhais, N., Cionni, I., Cortesi, N., Crezee, B., Davin, E. L., Davini, P., Debeire, K., de Mora, L., Deser, C., Docquier, D., Earnshaw, P., Ehbrecht,

465 C., Gier, B. K., Gonzalez-Reviriego, N., Goodman, P., Hagemann, S., Hardiman, S., Hassler, B., Hunter, A., Kadow, C., Kindermann, S., Koirala, S., Koldunov, N., Lejeune, Q., Lembo, V., Lovato, T., Lucarini, V., Massonnet, F., Muller, B., Pandde, A., Perez-Zanon, N., Phillips, A., Predoi, V., Russell, J., Sellar, A., Serva, F., Stacke, T., Swaminathan, R., Torralba, V., Vegas-Regidor, J., von Hardenberg, J., Weigel, K., and Zimmermann, K.: Earth System Model Evaluation Tool (ESMValTool) v2.0-an extended set of large-scale diagnostics for quasi-operational and comprehensive evaluation of Earth system models in CMIP, Geosci Model Dev, 13, 3383–3438,

470 https://doi.org/10.5194/gmd-13-3383-2020, 2020.

Frey, W. R. and Kay, J. E.: The influence of extratropical cloud phase and amount feedbacks on climate sensitivity, Climate Dynamics, 50, 3097–3116, https://doi.org/10.1007/s00382-017-3796-5, 2018.

Gent, P. R., Danabasoglu, G., Donner, L. J., Holland, M. M., Hunke, E. C., Jayne, S. R., Lawrence, D. M., Neale, R. B., Rasch, P. J., Vertenstein, M., Worley, P. H., Yang, Z. L., and Zhang, M. H.: The Community Climate System Model Version 4, J Climate, 24, 4973–

475 4991, https://doi.org/10.1175/2011jcli4083.1, 2011.

Gettelman, A., Hannay, C., Bacmeister, J. T., Neale, R. B., Pendergrass, A. G., Danabasoglu, G., Lamarque, J. F., Fasullo, J. T., Bailey, D. A., Lawrence, D. M., and Mills, M. J.: High Climate Sensitivity in the Community Earth System Model Version 2 (CESM2), Geophys Res Lett, 46, 8329–8337, https://doi.org/10.1029/2019gl083978, 2019.

Giorgetta, M. A., Jungclaus, J., Reick, C. H., Legutke, S., Bader, J., Bottinger, M., Brovkin, V., Crueger, T., Esch, M., Fieg, K., Glushak,

480 K., Gayler, V., Haak, H., Hollweg, H. D., Ilyina, T., Kinne, S., Kornblueh, L., Matei, D., Mauritsen, T., Mikolajewicz, U., Mueller, W., Notz, D., Pithan, F., Raddatz, T., Rast, S., Redler, R., Roeckner, E., Schmidt, H., Schnur, R., Segschneider, J., Six, K. D., Stockhause, M., Timmreck, C., Wegner, J., Widmann, H., Wieners, K. H., Claussen, M., Marotzke, J., and Stevens, B.: Climate and carbon cycle changes from 1850 to 2100 in MPI-ESM simulations for the Coupled Model Intercomparison Project phase 5, J Adv Model Earth Sy, 5, 572–597, https://doi.org/10.1002/Jame.20038, 2013.

485 Gregory, J. M., Ingram, W., Palmer, M., Jones, G., Stott, P., Thorpe, R., Lowe, J., Johns, T., and Williams, K. J. G. R. L.: A new method for diagnosing radiative forcing and climate sensitivity, Geophysical research letters, 31, 2004.

Hajima, T., Watanabe, M., Yamamoto, A., Tatebe, H., Noguchi, M. A., Abe, M., Ohgaito, R., Ito, A., Yamazaki, D., Okajima, H., Ito, A., Takata, K., Ogochi, K., Watanabe, S., and Kawamiya, M.: Development of the MIROC-ES2L Earth system model and the evaluation of biogeochemical processes and feedbacks, Geosci Model Dev Geosci Model Dev, 13, 2197–2244, 2020.

490 He, B., YU, Y., Bao, Q., Lin, P., Liu, H., Li, J., Wang, L., Liu, Y., Wu, G., Chen, K., Guo, Y., Zhao, S., Zhang, X., Song, M., and Xie, J.: CAS FGOALS-f3-L model dataset descriptions for CMIP6 DECK experiments, Atmospheric and Oceanic Science Letters, 13, 582–588, https://doi.org/10.1080/16742834.2020.1778419, 2020.

Hourdin, F., Grandpeix, J. Y., Rio, C., Bony, S., Jam, A., Cheruy, F., Rochetin, N., Fairhead, L., Idelkadi, A., Musat, I., Dufresne, J. L., Lahellec, A., Lefebvre, M. P., and Roehrig, R.: LMDZ5B: the atmospheric component of the IPSL climate model with revisited parameterizations for clouds and convection, Clim Dynam, 40, 2193–2222, https://doi.org/10.1007/s00382-012-1343-y, 2013.

Ji, D., Wang, L., Feng, J., Wu, Q., Cheng, H., Zhang, Q., Yang, J., Dong, W., Dai, Y., Gong, D., Zhang, R. H., Wang, X., Liu, J., Moore, J. C., Chen, D., and Zhou, M.: Description and basic evaluation of Beijing Normal University Earth System Model (BNU-ESM) version 1, Geosci Model Dev, 7, 2039–2064, https://doi.org/10.5194/gmd-7-2039-2014, 2014.

Jian, B., Li, J., Zhao, Y., He, Y., Wang, J., and Huang, J.: Evaluation of the CMIP6 planetary albedo climatology using satellite observations, Climate Dynamics, 54, 5145–5161, https://doi.org/10.1007/s00382-020-05277-4, 2020.

Jiang, J. H., Su, H., Wu, L., Zhai, C., and Schiro, K. A.: Improvements in Cloud and Water Vapor Simulations Over the Tropical Oceans in CMIP6 Compared to CMIP5, Earth and Space Science, 8, e2020EA001 520, https://doi.org/10.1029/2020EA001520, 2021.

Kato, S., Rose, F. G., Rutan, D. A., Thorsen, T. J., Loeb, N. G., Doelling, D. R., Huang, X., Smith, W. L., Su, W., and Ham, S.-H.: Surface Irradiances of Edition 4.0 Clouds and the Earth's Radiant Energy System (CERES) Energy Balanced and Filled (EBAF) Data Product, Journal of Climate, 31, 4501 – 4527, https://doi.org/10.1175/JCLI-D-17-0523.1, 2018.

Kelley, M., Schmidt, G. A., Nazarenko, L. S., Bauer, S. E., Ruedy, R., Russell, G. L., Ackerman, A. S., Aleinov, I., Bauer, M., Bleck, R., and others: GISS-E2. 1: Configurations and climatology, Journal of Advances in Modeling Earth Systems, 12, e2019MS002 025, publisher: Wiley Online Library, 2020.

Kuhlbrodt, T., Jones, C. G., Sellar, A., Storkey, D., Blockley, E., Stringer, M., Hill, R., Graham, T., Ridley, J., and Blaker, A.: The Low-Resolution Version of HadGEM3 GC3. 1: Development and Evaluation for Global Climate, Journal of advances in modeling earth systems, 10, 2865–2888, 2018.

Kuma, P., Bender, F. A.-M., Schuddeboom, A., McDonald, A. J., and Seland, O.: Machine learning of cloud types in satellite observations and climate models, Atmospheric Chemistry and Physics, 23, 523–549, https://doi.org/10.5194/acp-23-523-2023, 2023.

Lauer, A. and Hamilton, K.: Simulating Clouds with Global Climate Models: A Comparison of CMIP5 Results with CMIP3 and Satellite Data, Journal of Climate, 26, 3823 – 3845, https://doi.org/10.1175/JCLI-D-12-00451.1, place: Boston MA, USA Publisher: American Meteorological Society, 2013.

Lauer, A., Eyring, V., Bellprat, O., Bock, L., Gier, B. K., Hunter, A., Lorenz, R., Pérez-Zanón, N., Righi, M., Schlund, M., Senftleben, D., Weigel, K., and Zechlau, S.: Earth System Model Evaluation Tool (ESMValTool) v2.0 – diagnostics for emergent constraints and future projections from Earth system models in CMIP, Geosci. Model Dev., 13, 4205–4228, https://doi.org/10.5194/gmd-13-4205-2020, 2020.

Lauer, A., Bock, L., Hassler, B., Schröder, M., and Stengel, M.: Cloud Climatologies from Global Climate Models – A Comparison of CMIP5 and CMIP6 Models with Satellite Data, Journal of Climate, 36, 281–311, https://doi.org/10.1175/JCLI-D-22-0181.1, 2023.

Lee, J., Kim, J., Sun, M.-A., Kim, B.-H., Moon, H., Sung, H. M., Kim, J., and Byun, Y.-H.: Evaluation of the Korea Meteorological Administration Advanced Community Earth-System model (K-ACE), Asia-Pacific Journal of Atmospheric Sciences, 56, 381–395, https://doi.org/10.1007/s13143-019-00144-7, section: 381, 2020a.

Lee, W. L., Wang, Y. C., Shiu, C. J., Tsai, I. C., Tu, C. Y., Lan, Y. Y., Chen, J. P., Pan, H. L., and Hsu, H. H.: Taiwan Earth System Model Version 1: description and evaluation of mean state, Geosci Model Dev Geosci Model Dev, 13, 3887–3904, 2020b.

Lelli, L., Vountas, M., Khosravi, N., and Burrows, J. P.: Satellite remote sensing of regional and seasonal Arctic cooling showing a multi-decadal trend towards brighter and more liquid clouds, Atmospheric Chemistry and Physics, 23, 2579–2611, https://doi.org/10.5194/acp-23-2579-2023, 2023.

530 Li, L., Lin, P., Yu, Y., Wang, B., Zhou, T., Liu, L., Liu, J., Bao, Q., Xu, S., Huang, W., Xia, K., Pu, Y., Dong, L., Shen, S., Liu, Y., Hu, N., Liu, M., Sun, W., Shi, X., Zheng, W., Wu, B., Song, M.-R., Liu, H., Zhang, X., Wu, G., Xue, W., Huang, X., Yang, G., Song, Z., and Qiao, F.: The Flexible Global Ocean-Atmosphere-Land System Model version g2, Adv. Atmos. Sci., in press, https://doi.org/10.1007/s00376-012-2140-6, 2013.

Li, L. J., Yu, Y. Q., Tang, Y. L., Lin, P. F., Xie, J. B., Song, M. R., Dong, L., Zhou, T. J., Liu, L., Wang, L., Pu, Y., Chen, X. L., Chen, L., Xie,
535 Z. H., Liu, H. B., Zhang, L. X., Huang, X., Feng, T., Zheng, W. P., Xia, K., Liu, H. L., Liu, J. P., Wang, Y., Wang, L. H., Jia, B. H., Xie, F., Wang, B., Zhao, S. W., Yu, Z. P., Zhao, B. W., and Wei, J. L.: The Flexible Global Ocean-Atmosphere-Land System Model Grid-Point Version 3 (FGOALS-g3): Description and Evaluation, J Adv Model Earth Sy, 12, 2020.

Loeb, N. and NCAR Staff: The Climate Data Guide: CERES EBAF: Clouds and Earth's Radiant Energy Systems (CERES) Energy Balanced and Filled (EBAF), https://climatedataguide.ucar.edu/climate-data/
540 ceres-ebaf-clouds-and-earths-radiant-energy-systems-ceres-energy-balanced-and-filled, (last access on 2023-11-23), 2022.

Loeb, N. G., Doelling, D. R., Wang, H., Su, W., Nguyen, C., Corbett, J. G., Liang, L., Mitrescu, C., Rose, F. G., and Kato, S.: Clouds and the Earth's Radiant Energy System (CERES) Energy Balanced and Filled (EBAF) Top-of-Atmosphere (TOA) Edition-4.0 Data Product, Journal of Climate, 31, 895 – 918, https://doi.org/10.1175/JCLI-D-17-0208.1, 2018.

Mauritsen, T., Bader, J., Becker, T., Behrens, J., Bittner, M., Brokopf, R., Brovkin, V., Claussen, M., Crueger, T., Esch, M., Fast, I., Fiedler,
545 S., Flaeschner, D., Gayler, V., Giorgetta, M., Goll, D. S., Haak, H., Hagemann, S., Hedemann, C., Hohenegger, C., Ilyina, T., Jahns, T., Jimenez-de-la Cuesta, D., Jungclaus, J., Kleinen, T., Kloster, S., Kracher, D., Kinne, S., Kleberg, D., Lasslop, G., Kornblueh, L., Marotzke, J., Matei, D., Meraner, K., Mikolajewicz, U., Modali, K., Mobis, B., Muller, W. A., Nabel, J. E. M. S., Nam, C. C. W., Notz, D., Nyawira, S. S., Paulsen, H., Peters, K., Pincus, R., Pohlmann, H., Pongratz, J., Popp, M., Raddatz, T. J., Rast, S., Redler, R., Reick, C. H., Rohrschneider, T., Schemann, V., Schmidt, H., Schnur, R., Schulzweida, U., Six, K. D., Stein, L., Stemmler, I., Stevens, B., von Storch,
550 J. S., Tian, F. X., Voigt, A., Vrese, P., Wieners, K. H., Wilkenskjeld, S., Winkler, A., and Roeckner, E.: Developments in the MPI-M Earth System Model version 1.2 (MPI-ESM1.2) and Its Response to Increasing CO2, J Adv Model Earth Sy J Adv Model Earth Sy, 11, 998–1038, 2019.

Meehl, G. A., Senior, C. A., Eyring, V., Flato, G., Lamarque, J. F., Stouffer, R. J., Taylor, K. E., and Schlund, M.: Context for interpreting equilibrium climate sensitivity and transient climate response from the CMIP6 Earth system models, Sci Adv, 6, eaba1981,
555 https://doi.org/10.1126/sciadv.aba1981, edition: 2020/07/09, 2020.

Mizuta, R., Yoshimura, H., Murakami, H., Matsueda, M., Endo, H., Ose, T., Kamiguchi, K., Hosaka, M., Sugi, M., Yukimoto, S., and others: Climate simulations using MRI-AGCM3. 2 with 20-km grid, Journal of the Meteorological Society of Japan. Ser. II, 90, 233–258, publisher: Meteorological Society of Japan, 2012.

Muller, W. A., Jungclaus, J. H., Mauritsen, T., Baehr, J., Bittner, M., Budich, R., Bunzel, F., Esch, M., Ghosh, R., Haak, H., Ilyina, T.,
560 Kleine, T., Kornblueh, L., Li, H., Modali, K., Notz, D., Pohlmann, H., Roeckner, E., Stemmler, I., Tian, F., and Marotzke, J.: A Higher-resolution Version of the Max Planck Institute Earth System Model (MPI-ESM1.2-HR), J Adv Model Earth Sy J Adv Model Earth Sy, 10, 1383–1413, 2018.

Righi, M., Andela, B., Eyring, V., Lauer, A., Predoi, V., Schlund, M., Vegas-Regidor, J., Bock, L., Brötz, B., de Mora, L., Diblen, F., Dreyer, L., Drost, N., Earnshaw, P., Hassler, B., Koldunov, N., Little, B., Loosveldt Tomas, S., and Zimmermann, K.: Earth System Model
565 Evaluation Tool (ESMValTool) v2.0 – technical overview, Geosci. Model Dev., 13, 1179–1199, https://doi.org/10.5194/gmd-13-1179-2020, 2020.

Rong, X. Y., Li, J., Chen, H. M., Xin, Y. F., Su, J. Z., Hua, L. J., Zhou, T. J., Qi, Y. J., Zhang, Z. Q., Zhang, G., and Li, J. D.: The CAMS Climate System Model and a Basic Evaluation of Its Climatology and Climate Variability Simulation, J Meteorol Res-Prc J Meteorol Res-Prc, 32, 839–861, 2018.

570 Rotstayn, L. D., Collier, M. A., Dix, M. R., Feng, Y., Gordon, H. B., O'Farrell, S. P., Smith, I. N., and Syktus, J.: Improved simulation of Australian climate and ENSO-related rainfall variability in a global climate model with an interactive aerosol treatment, Int J Climatol, 30, 1067–1088, https://doi.org/10.1002/joc.1952, 2010.

Schlund, M., Lauer, A., Gentine, P., Sherwood, S. C., and Eyring, V.: Emergent constraints on Equilibrium Climate Sensitivity in CMIP5: do they hold for CMIP6?, Earth Syst. Dynam. Discuss., 2020, 1–40, https://doi.org/10.5194/esd-2020-49, 2020.

575 Schlund, M., Hassler, B., Lauer, A., Andela, B., Jöckel, P., Kazeroni, R., Loosveldt Tomas, S., Medeiros, B., Predoi, V., Sénési, S., Servonnat, J., Stacke, T., Vegas-Regidor, J., Zimmermann, K., and Eyring, V.: Evaluation of native Earth system model output with ESMValTool v2.6.0, Geoscientific Model Development, 16, 315–333, https://doi.org/10.5194/gmd-16-315-2023, 2023.

Schmidt, G. A., Ruedy, R., Hansen, J. E., Aleinov, I., Bell, N., Bauer, M., Bauer, S., Cairns, B., Canuto, V., Cheng, Y., Del Genio, A., Faluvegi, G., Friend, A. D., Hall, T. M., Hu, Y. Y., Kelley, M., Kiang, N. Y., Koch, D., Lacis, A. A., Lerner, J., Lo, K. K., Miller, R. L.,

580 Nazarenko, L., Oinas, V., Perlwitz, J., Perlwitz, J., Rind, D., Romanou, A., Russell, G. L., Sato, M., Shindell, D. T., Stone, P. H., Sun, S., Tausnev, N., Thresher, D., and Yao, M. S.: Present-day atmospheric simulations using GISS ModelE: Comparison to in situ, satellite, and reanalysis data, J Climate, 19, 153–192, https://doi.org/10.1175/Jcli3612.1, 2006.

Seland, O., Bentsen, M., Olivie, D., Toniazzo, T., Gjermundsen, A., Graff, L. S., Debernard, J. B., Gupta, A. K., He, Y. C., Kirkevag, A., Schwinger, J., Tjiputra, J., Aas, K. S., Bethke, I., Fan, Y. C., Griesfeller, J., Grini, A., Guo, C. C., Ilicak, M., Karset, I. H. H., Landgren, O.,

585 Liakka, J., Moseid, K. O., Nummelin, A., Spensberger, C., Tang, H., Zhang, Z. S., Heinze, C., Iversen, T., and Schulz, M.: Overview of the Norwegian Earth System Model (NorESM2) and key climate response of CMIP6 DECK, historical, and scenario simulations, Geosci Model Dev Geosci Model Dev, 13, 6165–6200, 2020.

Sellar, A. A., Jones, C. G., Mulcahy, J., Tang, Y., Yool, A., Wiltshire, A., O'connor, F. M., Stringer, M., Hill, R., and Palmieri, J.: UKESM1: Description and evaluation of the UK Earth System Model, Journal of Advances in Modeling Earth Systems, 2019.

590 Stevens, B., Giorgetta, M., Esch, M., Mauritsen, T., Crueger, T., Rast, S., Salzmann, M., Schmidt, H., Bader, J., Block, K., Brokopf, R., Fast, I., Kinne, S., Kornblueh, L., Lohmann, U., Pincus, R., Reichler, T., and Roeckner, E.: Atmospheric component of the MPI-M Earth System Model: ECHAM6, J Adv Model Earth Sy, 5, 146–172, https://doi.org/10.1002/jame.20015, 2013.

Swart, N. C., Cole, J. N., Kharin, V. V., Lazare, M., Scinocca, J. F., Gillett, N. P., Anstey, J., Arora, V., Christian, J. R., and Hanna, S.: The Canadian Earth System Model version 5 (CanESM5. 0.3), Geoscientific Model Development, 12, 4823–4873, 2019.

595 Séférian, R., Nabat, P., Michou, M., Saint-Martin, D., Voldoire, A., Colin, J., Decharme, B., Delire, C., Berthet, S., Chevallier, M., Sénési, S., Franchisteguy, L., Vial, J., Mallet, M., Joetzjer, E., Geoffroy, O., Guérémy, J.-F., Moine, M.-P., Msadek, R., Ribes, A., Rocher, M., Roehrig, R., Salas-y Mélia, D., Sanchez, E., Terray, L., Valcke, S., Waldman, R., Aumont, O., Bopp, L., Deshayes, J., Éthé, C., and Madec, G.: Evaluation of CNRM Earth System Model, CNRM-ESM2-1: Role of Earth System Processes in Present-Day and Future Climate, Journal of Advances in Modeling Earth Systems, n/a, https://doi.org/10.1029/2019ms001791, 2019.

600 Tatebe, H., Ogura, T., Nitta, T., Komuro, Y., Ogochi, K., Takemura, T., Sudo, K., Sekiguchi, M., Abe, M., Saito, F., Chikira, M., Watanabe, S., Mori, M., Hirota, N., Kawatani, Y., Mochizuki, T., Yoshimura, K., Takata, K., O'ishi, R., Yamazaki, D., Suzuki, T., Kurogi, M., Kataoka, T., Watanabe, M., and Kimoto, M.: Description and basic evaluation of simulated mean state, internal variability, and climate sensitivity in MIROC6, Geosci Model Dev Geosci Model Dev, 12, 2727–2765, 2019.

Taylor, K. E., Stouffer, R. J., and Meehl, G. A.: An overview of CMIP5 and the experiment design, Bulletin of the American Meteorological Society, 93, 485–498, 2012.

Voldoire, A., Saint-Martin, D., Senesi, S., Decharme, B., Alias, A., Chevallier, M., Colin, J., Gueremy, J. F., Michou, M., Moine, M. P., Nabat, P., Roehrig, R., Melia, D. S. Y., Seferian, R., Valcke, S., Beau, I., Belamari, S., Berthet, S., Cassou, C., Cattiaux, J., Deshayes, J., Douville, H., Ethe, C., Franchisteguy, L., Geoffroy, O., Levy, C., Madec, G., Meurdesoif, Y., Msadek, R., Ribes, A., Sanchez-Gomez, E., Terray, L., and Waldman, R.: Evaluation of CMIP6 DECK Experiments With CNRM-CM6-1, J Adv Model Earth Sy J Adv Model Earth Sy, 11, 2177–2213, 2019.

Volodin, E. M., Dianskii, N. A., and Gusev, A. V.: Simulating present-day climate with the INMCM4.0 coupled model of the atmospheric and oceanic general circulations, Izv Atmos Ocean Phy+, 46, 414–431, https://doi.org/10.1134/S000143381004002x, 2010.

Watanabe, M., Suzuki, T., O'ishi, R., Komuro, Y., Watanabe, S., Emori, S., Takemura, T., Chikira, M., Ogura, T., Sekiguchi, M., Takata, K., Yamazaki, D., Yokohata, T., Nozawa, T., Hasumi, H., Tatebe, H., and Kimoto, M.: Improved Climate Simulation by MIROC5. Mean States, Variability, and Climate Sensitivity, J Climate, 23, 6312–6335, https://doi.org/10.1175/2010JCLI3679.1, 2010.

Watanabe, S., Hajima, T., Sudo, K., Nagashima, T., Takemura, T., Okajima, H., Nozawa, T., Kawase, H., Abe, M., Yokohata, T., Ise, T., Sato, H., Kato, E., Takata, K., Emori, S., and Kawamiya, M.: MIROC-ESM 2010: model description and basic results of CMIP5-20c3m experiments, Geosci Model Dev, 4, 845–872, https://doi.org/10.5194/gmd-4-845-2011, 2011.

Weigel, K., Bock, L., Gier, B. K., Lauer, A., Righi, M., Schlund, M., Adeniyi, K., Andela, B., Arnone, E., Berg, P., Caron, L.-P., Cionni, I., Corti, S., Drost, N., Hunter, A., Lledó, L., Mohr, C. W., Paçal, A., Pérez-Zanón, N., Predoi, V., Sandstad, M., Sillmann, J., Sterl, A., Vegas-Regidor, J., von Hardenberg, J., and Eyring, V.: Earth System Model Evaluation Tool (ESMValTool) v2.0 – diagnostics for extreme events, regional and impact evaluation, and analysis of Earth system models in CMIP, Geoscientific Model Development, 14, 3159–3184, https://doi.org/10.5194/gmd-14-3159-2021, 2021.

Williams, K. D., Copsey, D., Blockley, E. W., Bodas-Salcedo, A., Calvert, D., Comer, R., Davis, P., Graham, T., Hewitt, H. T., Hill, R., Hyder, P., Ineson, S., Johns, T. C., Keen, A. B., Lee, R. W., Megann, A., Milton, S. F., Rae, J. G. L., Roberts, M. J., Scaife, A. A., Schiemann, R., Storkey, D., Thorpe, L., Watterson, I. G., Walters, D. N., West, A., Wood, R. A., Woollings, T., and Xavier, P. K.: The Met Office Global Coupled Model 3.0 and 3.1 (GC3.0 and GC3.1) Configurations, Journal of Advances in Modeling Earth Systems, 10, 357–380, https://doi.org/10.1002/2017ms001115, 2018.

Wu, T. W.: A mass-flux cumulus parameterization scheme for large-scale models: description and test with observations, Clim Dynam, 38, 725–744, https://doi.org/10.1007/s00382-011-0995-3, 2012.

Wu, T. W., Yu, R. C., Zhang, F., Wang, Z. Z., Dong, M., Wang, L. N., Jin, X., Chen, D. L., and Li, L.: The Beijing Climate Center atmospheric general circulation model: description and its performance for the present-day climate, Clim Dynam, 34, 123–147, https://doi.org/10.1007/s00382-008-0487-2, 2010.

Wu, T. W., Lu, Y. X., Fang, Y. J., Xin, X. G., Li, L., Li, W. P., Jie, W. H., Zhang, J., Liu, Y. M., Zhang, L., Zhang, F., Zhang, Y. W., Wu, F. H., Li, J. L., Chu, M., Wang, Z. Z., Shi, X. L., Liu, X. W., Wei, M., Huang, A. N., Zhang, Y. C., and Liu, X. H.: The Beijing Climate Center Climate System Model (BCC-CSM): the main progress from CMIP5 to CMIP6, Geosci Model Dev Geosci Model Dev, 12, 1573–1600, 2019.

Yukimoto, S., Adachi, Y., Hosaka, M., Sakami, T., Yoshimura, H., Hirabara, M., Tanaka, T. Y., Shindo, E., Tsujino, H., Deushi, M., Mizuta, R., Yabu, S., Obata, A., Nakano, H., Koshiro, T., Ose, T., and Kitoh, A.: A New Global Climate Model of the Meteorological Research Institute: MRI-CGCM3-Model Description and Basic Performance, J Meteorol Soc Jpn, 90a, 23–64, https://doi.org/10.2151/jmsj.2012-A02, 2012.

Yukimoto, S., Kawai, H., Koshiro, T., Oshima, N., Yoshida, K., Urakawa, S., Tsujino, H., Deushi, M., Tanaka, T., Hosaka, M., Yabu, S., Yoshimura, H., Shindo, E., Mizuta, R., Obata, A., Adachi, Y., and Ishii, M.: The Meteorological Research Institute Earth System Model Version 2.0, MRI-ESM2.0: Description and Basic Evaluation of the Physical Component, J Meteorol Soc Jpn J Meteorol Soc Jpn, 97, 931–965, 2019.

Zelinka, M. D., Myers, T. A., Mccoy, D. T., Po-Chedley, S., Caldwell, P. M., Ceppi, P., Klein, S. A., and Taylor, K. E.: Causes of Higher Climate Sensitivity in CMIP6 Models, Geophys Res Lett, 47, https://doi.org/10.1029/2019GL085782, 2020.

Zhu, J., Otto-Bliesner, B. L., Brady, E. C., Gettelman, A., Bacmeister, J. T., Neale, R. B., Poulsen, C. J., Shaw, J. K., McGraw, Z. S., and Kay, J. E.: LGM Paleoclimate Constraints Inform Cloud Parameterizations and Equilibrium Climate Sensitivity in CESM2, Journal of Advances in Modeling Earth Systems, 14, e2021MS002 776, https://doi.org/10.1029/2021MS002776, 2022.